universität wien

MASTERARBEIT | MASTER'S THESIS

Titel | Title

Esterified oxylipin analysis in human cancer cell lines

verfasst von | submitted by

Konstantin Kaltenböck BSc

angestrebter akademischer Grad | in partial fulfilment of the requirements for the degree of

Master of Science (MSc)

Wien | Vienna, 2024

Studienkennzahl lt. Studienblatt | Degree programme code as it appears on the student record sheet:	UA 066 863
Studienrichtung lt. Studienblatt | Degree programme as it appears on the student record sheet:	Masterstudium Biologische Chemie
Betreut von | Supervisor:	Ass.-Prof. Dr. Samuel Matthias Meier-Menches Privatdoz. BSc MSc

Acknowledgements

First and foremost, I want to express my utmost gratitude towards my supervisor Ass.-Prof. Dr. Samuel Meier Menches, who gave me the opportunity to join his group and work on a fascinating topic where I could implement my own ideas, and who mentored me throughout this project, always providing encouragement in challenging times. I would also like to thank Univ.-Prof. Dr. Christopher Gerner for his professional guidance, consultation and inspiration.

Further I would to thank Dr. Gerhard Hagn for his personal and professional guidance and support throughout this project which were crucial for this thesis. Also, I would like to thank Yasmin Borutzki and Lukas Skos, for their introduction to the cell culture laboratory techniques and their guidance during the experiments, providing me with their invaluable advice and experience. Then, I would like to pay my special regards to Michael Wolf and Hanna Troiss for their support in data acquisition and extraction.

My sincere appreciation goes out to every member of the research groups of Univ.-Prof. Dr. Christopher Gerner and Ass.-Prof. Dr. Samuel Meier Menches, for their warm welcome, their inspiring conversations and their contributions to this project.

Lastly, I would like to thank my family and loved ones for their unconditional support during my educational journey.

Zusammenfassung

Oxylipine, die Oxidationsprodukte mehrfach ungesättigter Fettsäuren, sind eine Gruppe bioaktiver Fettsäurederivate. Während bereits große Anstrengungen zur Charakterisierung von ungebundenen Oxylipinen unternommen wurden, ist die Zusammensetzung ihrer membrangebundenen Fraktion noch wenig erforscht. In dieser Arbeit wurde eine auf Verseifung basierende Extraktionsmethode für die ungezielte LC-MS-Analyse von membrangebundenen Oxylipinen in menschlichen Krebszelllinien erfolgreich eingesetzt und optimiert. Eine Zelldichte von 10^5 Zellen pro Probe und eine Verseifungszeit von 30 Minuten wurden als optimale Bedingungen für diese Methode ermittelt, um die Analyt- und Standardvariationen zu minimieren. Die Methode wurde zunächst zur Charakterisierung der Fettsäure- und Oxylipinprofile der promyelozytären Zelllinie HL-60 nach Behandlung mit all-trans-Retinsäure (ATRA) und Dimethylsulfoxid (DMSO) unter Stimulation durch den transformierenden Wachstumsfaktor beta 1 (TGF-β1) eingesetzt. In HL-60-Zellen unter ATRA-Behandlung verursachte die TGF-β1-Stimulation eine Hochregulierung von 18-HETE. Die DMSO-Behandlung führte zu einem Gesamtrückgang fast aller Analyten, was möglicherweise auf eine Membranausdünnung zurückzuführen ist. Des Weiteren wurden die Auswirkungen des regulierten Zelltods in der Eierstockkrebs-Zelllinie A2780 auf das Fettsäure- und Oxylipinprofil in zellulären und mitochondrialen Fraktionen untersucht. Im Einzelnen wurden die Cisplatin-induzierte Apoptose und die RSL3-induzierte Ferroptose untersucht. In ferroptotischen A2780 Zelllysaten wurde festgestellt, dass 14,15-DiHETrE, 11,12-DiHETrE und 14-HEPE signifikant hochreguliert und 20-HEPE herunterreguliert waren. In mitochondrialen Lysaten wurde eine Hochregulierung von 14(15)-DiHETE festgestellt. Weiters wurde ein Synergismus-Test zwischen RSL3 und NDGA durchgeführt, der starke antagonistische Effekte des 5-LOX-Inhibitors NDGA auf die Wirkung von RSL3 ergab. Die Untersuchung des membrangebundenen Oxylipin- und Fettsäureprofils unter diesem antagonistischen Zustand ergab außerdem einen signifikanten Rückgang der 18-HEPE- und 5(6)-EET-Niveaus im Vergleich zu unbehandelten Kontrollzellen und Zellen, die nur mit RSL3 behandelt wurden. Die in dieser Arbeit beschriebene, auf

Verseifung basierende Extraktion von membrangebundenen Fettsäuren und Oxylipinen bietet eine zuverlässige Methode für deren Charakterisierung und, die für zukünftige molekulare Charakterisierungen biologischer Membranen hilfreich sein kann.

Abstract

Oxylipins are a group of bioactive fatty acid derivates and products of the oxidation of poly-unsaturated fatty acids. While great effort has already been put into the characterization of oxylipins, the characterization of the composition of their membrane bound fraction remains under-investigated. In this thesis a saponification-based extraction method for untargeted LC-MS analysis of membrane-bound oxylipins in human cancer cell lines was successfully adopted and optimized. A cell density of 10^5 cells per sample and a saponification time of 30 min was identified as optimal conditions for this method to minimize analyte and standard variation. The method was firstly implemented to characterize fatty acid and oxylipin profiles of the promyelocytic cell line HL-60 upon treatment with all-*trans* retinoic acid (ATRA) and dimethyl sulfoxide (DMSO) under stimulation with transforming growth factor beta 1 (TGF-β1). In HL-60 cells under ATRA treatment, TGF-β1 stimulation caused an upregulation of 18-HETE. DMSO treatment led to an overall decrease of almost every analyte which is potentially caused by membrane thinning. Further, the impact of regulated cell death in the ovarian cancer cell line A2780 on the fatty acid and oxylipin profile in cellular and mitochondrial fractions was studied. In detail, Cisplatin-induced apoptosis, and RSL3-induced ferroptosis were investigated. The former is expected to be executed by caspases with a minor effect on lipids, while the latter is driven by lipid peroxidation. In ferroptotic A2780 whole cell lysates 14,15-DiHETrE, 11,12-DiHETrE and 14-HEPE were found to be significantly upregulated and 20-HEPE was down-regulated. In mitochondrial lysates, 14(15)-DiHETE was found to be upregulated. Lastly, a synergism assay between RSL3 and NDGA was performed which revealed strong antagonistic effects of the 5-LOX inhibitor NDGA on RSL3. The investigation of the membrane bound oxylipin and fatty acid profile under this antagonistic state further revealed a significant decrease of 18-HEPE and 5(6)-EET levels in comparison to both untreated control cells and cells treated with RSL3 only. The saponification-based extraction of membrane-bound fatty acids and oxylipins described in this thesis provides a reliable method for their characterization and will be helpful for future molecular characterizations of biological membranes.

Table of Contents

1. Introduction

1.1 Oxylipins

Oxylipins are a group of oxidation products from poly unsaturated fatty acids (PUFAs) acting as mediators for multiple physiological processes[1], including inflammation regulation[2], activation of membrane permeability[3], and tumor growth promotion[4]. Oxylipin levels depend on the physiological status and can be altered in response to inflammation[5], nutrition[6] pharmaceutical intervention[7] and cell death initiation[3] among others. The bioactive functions of oxylipins were first characterized in the 1930s. It was discovered that the contractile function of seminal fluids on uterine tissues was also present in alkaline oil extracts of the fluids indicating the existence of bioactive fatty acids that were coined as prostaglandins[8]. In 1982, the Nobel Prize in Medicine was awarded to Bengt Samuelsson, Sune Bergrström and John Vane for their research conducted during the 1960s and 1970s on oxylipins[9]. Initially, Samuelsson and Bergström elucidated the structure of prostaglandins and demonstrated that they are derived from the PUFA arachidonic acid[10]. Subsequently, they identified the biosynthetic pathway involving the enzymatic oxidation of PUFAs[11]. This enabled Vane's discovery that the therapeutic effects of aspirin can be attributed to its inhibition of prostaglandin formation[12].

1.1.1 Functions and biological relevance

The diversity of oxylipin functions can be attributed to their role as signaling molecules inherently acting on a wide range of physiological processes. To induce an effect, oxylipins can directly interact with receptors or by alteration of electrostatic interactions in membranes leading to a subsequent enzymatic metabolism. An example of a direct oxylipin-receptor induced function is the interaction between Leukotriene B_4 (LTB_4, illustrated in Figure 1) with Leukotriene B_4 receptor 1 (BLT1), a G-protein-coupled receptor (GPCR), inducing chemotaxis in myeloid leukocytes[13]. In promyeoloid HL-60

cells differentiated with all-trans retinoic acid (ATRA), an increased expression of BLT1 causes their migration towards LTB_4 secreting microglia[14]. A relevant example of an electrostatic alteration effect is the incorporation of oxylipins into membranes via the Land Cycle in which oxylipins are incorporated into phospholipids forming enzymatically oxidized phospholipids (eoxPLs)[15]. These eoxPLs, exert their functions via low affinity interactions with proteins or by changing the electronegativity of a membrane. An example of these functions are the changes in membrane structures upon activation of innate immune cells[15]. Oxylipins are furthermore involved in cell death signaling. The C18-oxylipins 9,10-DiHOME and 12,13-DiHOME (both illustrated in Figure 1) cause the permeabilization of the inner mitochondrial and subsequent release of cytochrome c into the cytosol[3]. When cytochrome c is released into the cytosol, it associates with apoptotic protease-activating factor 1 (Apaf-1) forming the apoptosome initiating apoptosis[16].

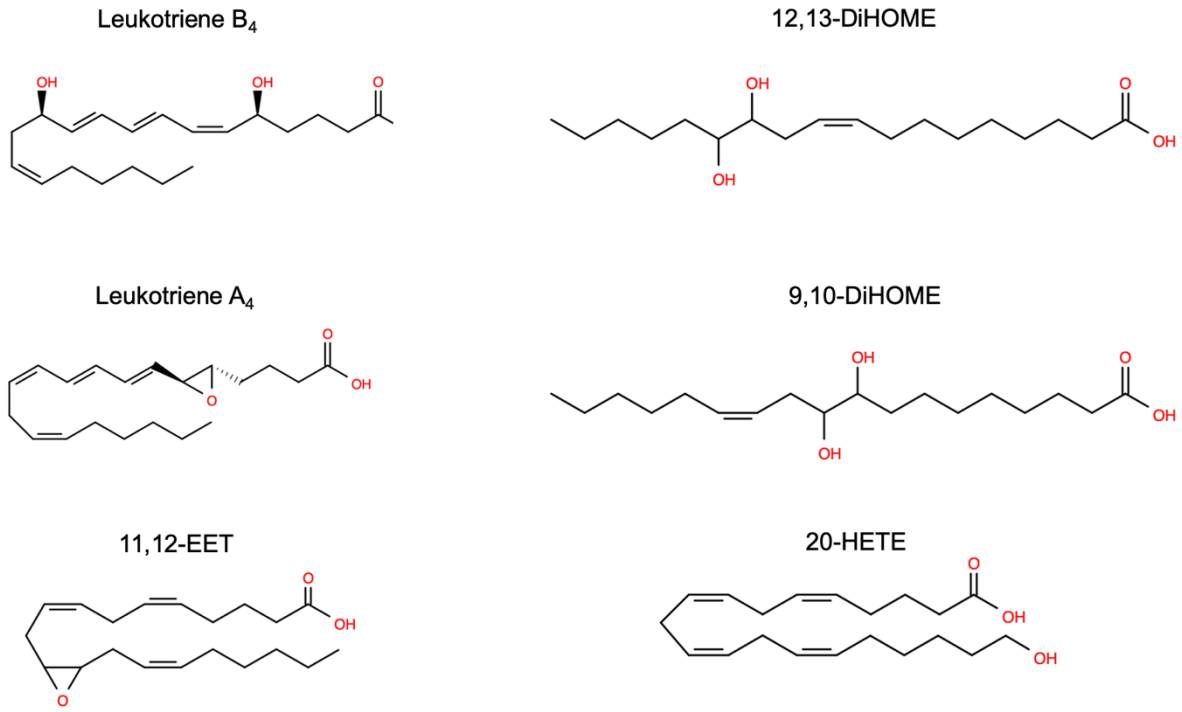

Figure 1: Examples of oxylipin structures. All molecular structures are retrieved from LIPID MAPS® [17]

1.1.2 Formation

The precursors of oxylipins are PUFAs. These include linoleic acid (LA, Ω6 C18:2), α-linoleic acid (ALA, Ω3 C18:3), dihomo-γ-linoleic acid (DGLA, Ω6 C20:3), arachidonic acid (AA, Ω6 C20:4), eicosapentaenoic acid (EPA, Ω3 C20:5) and adrenic acid (AdA, Ω6 C22:4)[1]. As constituents of cellular membranes, they are esterified to triglycerides that are linked to phosphates[18]. Cytostolic phospholipase 2 ($cPLA_2$) hydrolyses PUFAs from cell membranes upon an extracellular stimulus[19]. In addition to the oxidation of free PUFAs, esterified PUFAs can also be directly oxidized giving rise to esterified oxylipins[20]. The formation of oxylipins occurs either enzymatically via oxygenases[6] or by non-enzymatic autoxidation[21].

1.1.2.1 Cyclooxygenases

Cyclooxygenases 1 and 2 (COX-1 and COX-2) are hemoproteins with tyrosyl radicals that catalyze the oxidation of AA into prostaglandin H_2 (PGH_2), AdA into dihomo-PGH_2, EPA into PGH_3 and DGLA into PGH_1 [1,22]. COX-1 and COX-2 are 60% identical isoforms[23]. COX-1 is present in most tissues and responsible of prostaglandin production critical for autocrine and paracrine responses, maintenance of gastric mucosal integrity and platelet function[24]. COX-2 has a larger active site in comparison to COX-1 and can thereby interact with a larger variety of substrates. In contrast to COX-1 being mainly restricted to 20 carbon fatty acids, COX-2 can turn over 18-and 20 carbon fatty acids equally well[25]. COX-2 is expressed at inflammation sites and contributes to inflammatory response and regulation[26].

Formation of PGHs occurs via the formation of their respective PGG intermediates, that are formed via hydrogen abstraction and subsequent formation of an endoperoxide ring. In AA, COXs first abstract the L-pro(S) hydrogen at C_{13} and then oxygenate C_{11} from the antarafacial side forming an 11(R)-hydroperoxyl intermediate leading to the formation of a dioxabicycloheptane ring[27]. The mechanism of the COX mediated C_{13} hydrogen abstraction and C_{11} oxygenation and subsequent PGG formation is depicted in Figure 2.

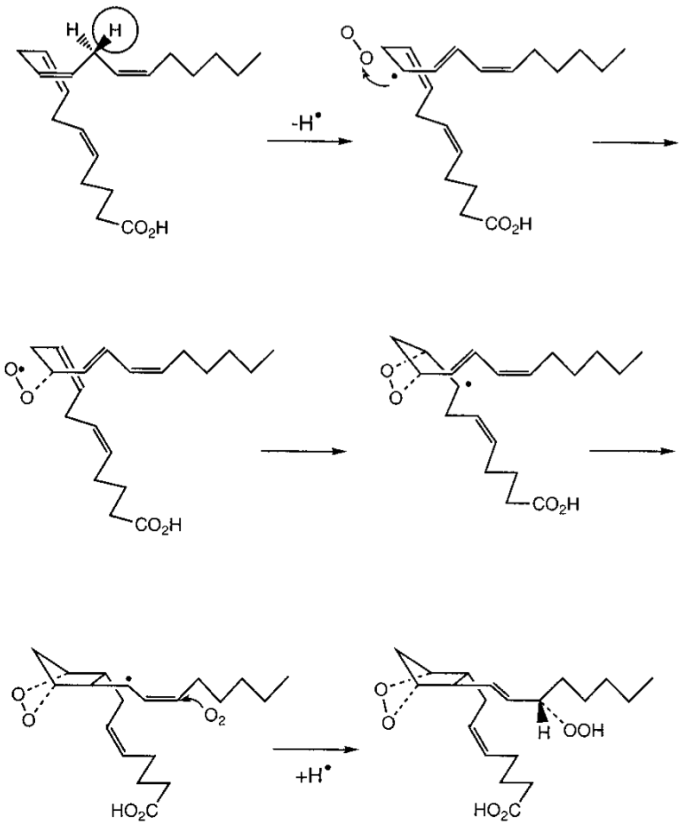

Figure 2: Reaction mechanism of COX-mediated PGG formation from AA[16]

PGGs are then converted into PGHs by the peroxidase activity of COX[28]. Tissue-specific isomerases then metabolize prostaglandin H into their respective prostaglandins and thromboxanes which then interact with specific G-protein coupled receptors[29].

1.1.2.2 Lipoxygenases

Lipoxygenases recognize 1Z,4Z pentadiene structures in PUFAs, incorporate oxygens and thereby generate hydroperoxy acids containing conjugated dienes at specific carbons of PUFAs[30,31]. Conventionally, the LOX isozymes are categorized according to the specific carbon, that is targeted in AA[32]. These are carbon 5, 8, 12 and 15 which are targeted by 5-LOX, 8-LOX 12-LOX and 15-LOX respectively[31]. Subsequent oxidations of a different LOX can also occur giving rise to PUFAs with several

hydroperoxy groups[30]. The resulting hydroperoxy-PUFA derivatives then serve as intermediates in the synthesis of a vast number of oxylipins. The hydroperoxides can undergo reduction via peroxidases to form hydroxides and further dehydration via dehydrogenases or cytochrome p450 to form ketones[33]. The oxidation of and subsequent reduction and dehydration steps of AA are illustrated in Figure 3 [33].

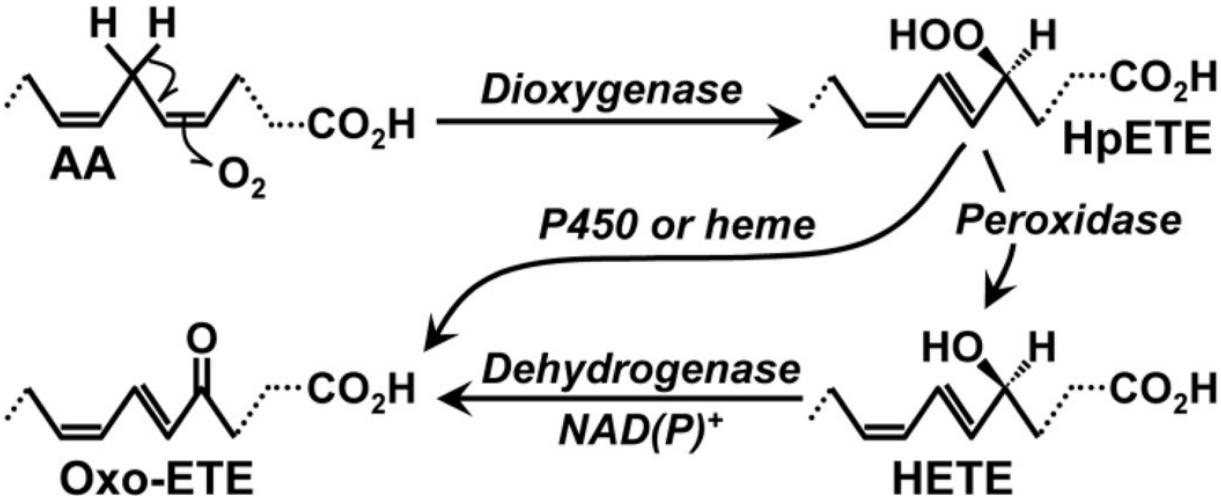

Figure 3: Oxidation of AA, subsequent reduction of hydroperoxides and formation of ketones in oxylipins[33]

In the case of 5-LOX, a subsequent second interaction with the PUFA-hydroperoxide leads to the formation of an epoxide and thereby the formation of leukotriene A_4 (LTA_4, illustrated in Figure 1)[34].

1.1.2.3 Cytochrome P45011

Human cytochrome P450 (CYP) is a superfamily of 57 enzyme subfamilies inducing oxidations, peroxidations and reductions in a wide variety of both endo- and exogenous compounds[35]. CYPs are important enzymes in the metabolism of PUFAs introducing epoxides and hydroxides. The subfamily CYP4 enzymes catalyze the hydroxylation of the terminal carbon in PUFAs[36]. The subfamily of CYP2 epoxygenases catalyze the epoxidation of all double bonds in PUFA. In the case of most CYP2 epoxygenases, the epoxidation is restricted to one or two specific loci[37]. The $G\alpha_s$ protein is a receptor interacting with an epoxide of AA, 11,12-epoxyeicosatrienoic acid (11,12-EET, illustrated in Figure 1), inducing vasodilation. PUFA-epoxides can influence signal

transduction pathways via interaction with the $G_s\alpha$ protein inducing vasodilation[38,39]. Several other functions are attributed to PUFA-epoxides including anti-inflammatory effects, vasodilation and fibrinolytic effects. The exact receptors involved in these functions however remain to be discovered[40]. PUFA-epoxides are furthermore substrates for soluble epoxide hydrolases catalyzing the hydration of epoxide yielding 2 neighboring hydroxides[41].

1.1.2.4 Non-enzymatic oxidation of PUFAs

Apart from enzymatically catalyzed oxidation, autooxidation of PUFAs through reactions with lipid radicals is another important source of oxylipins. The lipid radicals can either be induced exogenously by chemical reagents and physical stimuli like UV-light and ionizing radiation or endogenously as by-products of enzymatic activity or the mitochondrial electron transport chain[42]. After a lipid radical has formed, it can interact with molecular oxygen forming a peroxyl radical at partial pressures above 100 mmHg[42,43]. Subsequently, the peroxyl radical can abstract a hydrogen at an allylic or bis-allylic carbon of another PUFA molecule turning itself into an oxylipin and its substrate molecule into another lipid radical[44]. Alternatively, a peroxyl radical can form a bond with an alkene leading either to the formation of an epoxide by a subsequent homolytic substitution or react with another molecular oxygen to form another peroxyl radical[45]. This reaction proceeds until 2 radicals neutralize another[43]. In linear PUFAs, the radical intermediate is highly delocalized giving rise to a variety of possibly resulting oxylipin isomers[42]. PUFAs with at least 3 double bonds and an E,E diene conformation highly tend towards a cyclization after an oxidation giving rise to isoprostanes, isofuranes and serial cyclic peroxides[42,46]. After the formation of a peroxyl radical, a 5-oxo cyclization and subsequent oxidation occurs. At increased oxygen tension, the formation of isofuranes and serial cyclic peroxides is favored, while isoprostane formation at lower oxygen tension[46]. The non-enzymatic formation of cyclic oxylipins is illustrated in Figure 4 [46].

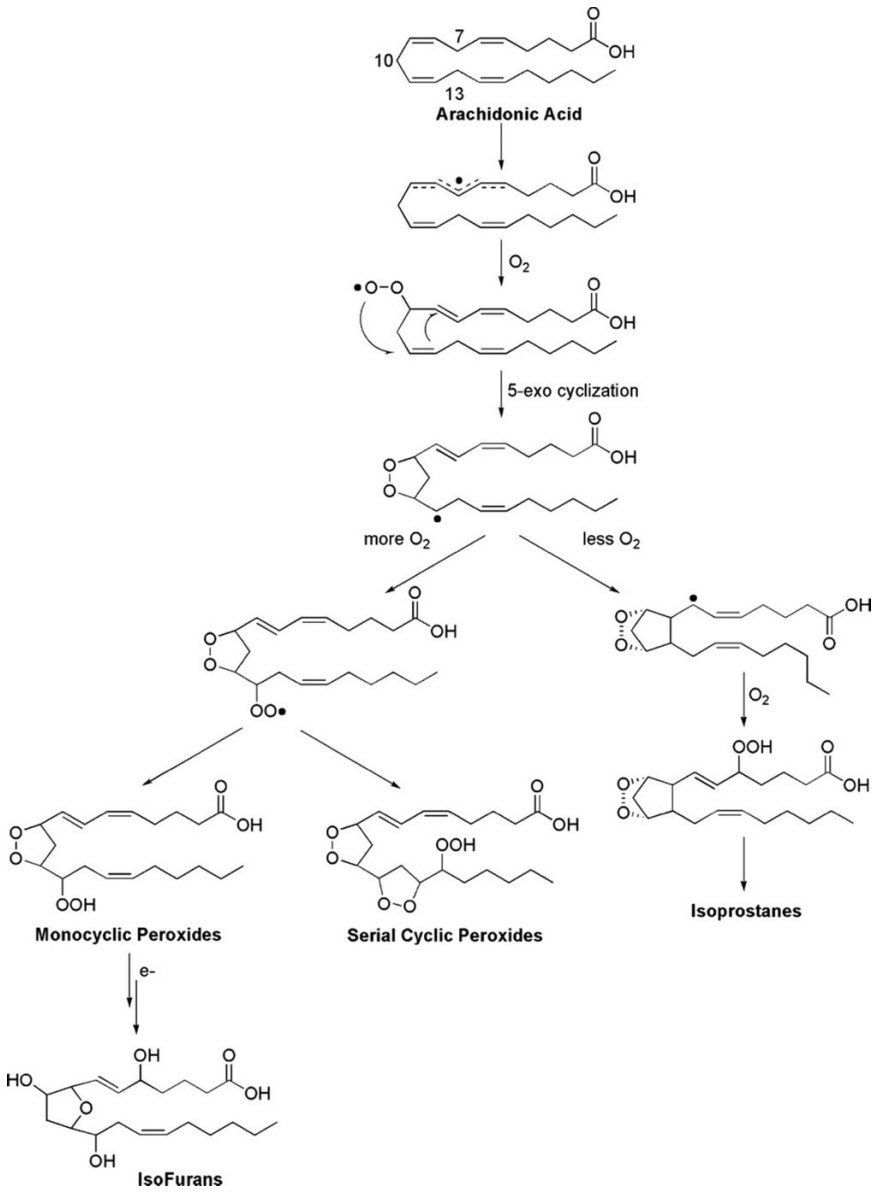

Figure 4: Non-enzymatic formation of cyclic oxylipins [46]

Isoprostanes are widely used as biomarkers for oxidative stress and likely are mediators in oxidant injuries[47]. Due to the increased formation of isofuranes at higher oxygen tensions, they might be a better indicator for oxidative stress[46].

1.1 Oxylipins in hematopoiesis

Oxylipins have shown to play a role in hematopoiesis. For instance, the CYP450 derived EETs interacts with GPR132, a G-protein coupled receptor that induces differentiation[48,49]. Myeloid cells are a class of blood cells originating from hematopoietic stem cells (HSCs) in the bone marrow[50]. This class of blood cells is comprised of granulocytes, monocytes, macrophages and dendritic cells. Myeloid cells are in the blood circulation and are deployed towards sites of tissue damage or infection via chemotaxis. At these sites, they are essential for protective immunity and phagocytosis. Furthermore, myeloid cells are involved in homeostasis and tissue repair[51]. HSCs are multipotent stem cells that can differentiate into all types of blood cells. Residing in the bone marrow, HSCs are essential for hematopoiesis. They are fully able to self-renew and give rise to several lines of oligopotent progenitors that further differentiate into mature blood cells[52]. Inflammations in the bone marrow can induce mutations in the HSCs the cause the impairment of hematopoietic differentiation leading to myeloid malignancies[53]. These can be treated effectively with differentiation induction chemotherapy using all-trans retinoic acid (ATRA)[54] or arsenic trioxide[55]. The promyelocytic leukemia cell line HL-60 is a commonly used model system to study myeloid differentiation. It is confined in its differentiation and can upon chemical treatment be differentiated into monocyte-, or granulocyte-like cells[56]. In HL-60 cells, a wide variety of compounds such as ATRA, dimethylformadie and dimethyl sulfoxide (DMSO) can be used to induce a differentiation into granulocyte-like cells[57]. Mechanistically, treatment with those agents induces the formation of neutrophil extracellular traps (NETs) that are characteristic for granulocytes[57]. HL-60 differentiation into granulocytes further causes changes in morphology, proliferation and adhesion properties[58].

1.3 Cell death

Cell death is a mechanism necessary in several fundamental processes of multicellular organisms including embryonic development, maintaining homeostasis and the elimination of damaged cells. Generally, cell death can be categorized into regulated cell death (RCD) and nonregulated cell death (non-RCD)[59]. Regulated cell death can occur as regulated necrosis through a targeted damage of the cell membrane via several effector mechanisms in the form of pyroptosis, necroptosis or ferroptosis[60]. Apoptosis allows the removal of a cell without the release of cytosolic material into the intracellular space preventing inflammatory responses, unlike lytic RCDs such as ferroptosis[61,62]. [60]

1.3.1 Apoptosis

Apoptosis is a noninflammatory, silent RCD that occurs in cells under physiological conditions[63]. The concept of apoptosis was first coined in 1972 in a project that studied the morphological changes of a cell during apoptosis which comprise of the formation of apoptotic bodies followed by the targeted phagocytosis by other cells[64]. Apoptosis is essential during gametogenesis and embryonic development but is also the cause of pathologic events such as carcinogenesis, AIDS, Parkinson disease and Alzheimer disease[65]. Furthermore, apoptosis is necessary for the maintenance of homeostasis keeping cell growth rates and cell death in balance and for a directed elimination of pathogenic cells such as infected cells, tumor cells and cells with substantial DNA damage[66]. Apoptosis can be induced through cell stress events such as damage of DNA and cytoskeleton, accumulation of unfolded proteins and the deprivation of cytokines among others. This induction pathway is frequently referred to as the mitochondrial pathway because the stress events lead to a permeabilization of the outer mitochondrial membrane and a subsequent release of cytochrome c into the cytosol. Cytochrome c then binds to Apaf-1 and procaspase-9 forming the apoptosome which activates caspase-9. Caspase-9 then cleaves procaspase-3 converting it into active caspase-3 which cleaves up to approximately 1300 cellular protein substrates to

execute apoptosis[67]. Notably, the mitochondrial pathway is an essential target for chemotherapeutic applications. Being among the most commonly used chemotherapeutic drug, cisplatin (illustrated in Figure 5) induces DNA damage by the introduction of covalent intrastrand crosslinks of the purine bases and thereby triggers the mitochondrial apoptosis pathway[68]. Alternatively, apoptosis can be induced by the death receptor pathway through the interaction between death ligands and receptors. The ligands are all closely related molecules of the tumor necrosis factor family (TNF), and the receptors form the family of tumor necrosis factor family receptors (TNFRs). In the case of the TNFR Fas, an interaction with its ligand causes a conformational change in Fas exposing its death domain. The death domain of Fas then interacts with the death domain of Fas associated death domain protein (FADD) leading to the formation of a Fas-FADD oligomer that recruits and oligomerizes caspase-8. The Caspase-8 oligomer then cleaves itself into active caspase-8 dimers that then cleave precaspase-3 and thereby activate caspase-3[69]. Among many other functions, caspase-3 cleaves flippases, that continuously ensure the asymmetric distribution of phosphatidylserine (PS) in the cell membrane. The inactivation of flippases causes the presence of PS on the outer surface of a cell. Phagocytes have receptors that detect PS, promote cell engulfment and phagocytosis[70].

1.3.2 Ferroptosis

Ferroptosis was first described in 2012 as an iron dependent form of RCD with distinct morphological, biochemical and genetic characteristics. During ferroptosis, cell death occurs due to an accumulation of lipid ROS[71]. It is strongly indicated, that the critical source of ROS for ferroptosis is LOX mediated oxidation since 5-LOX inhibitors such as Nordihydroguaiaretic acid (NDGA, Figure 5) are able to prevent ferroptotic death [72]. Further inhibitors of ferroptosis are inhibitors of PUFA peroxidation such as ferrostatins and Vitamin E[73]. While Vitamin E also acts as a 5-LOX inhibitor, ferrostatin-1 acts as a scavenger that traps peroxyl radicals[74,75]. Ferroptosis is induced, when the function of glutathione peroxidase 4 (GPX4) is disrupted. GPX4 is a selenoprotein that reduces lipid peroxides to lipid alcohols upon oxidation of the cofactor glutathione (GSH)[76]. The disruption of this redox system can be induced by intercepting the cystine supply essential for GSH synthesis through inhibition of the cystine glutamate antiporter system x_c^- with small molecules like erastin[77]. Alternatively, ferroptosis can be induced by inhibiting GPX4 with RSL3 (Figure 5), another small molecule that covalently binds to GPX4 and thereby inhibits it directly[78]. Further, there are oxylipins such as 20-HETE (illustrated in Figure 1) that acts directly as pro-ferroptotic agent by decreasing the expression of GPX-4[79].

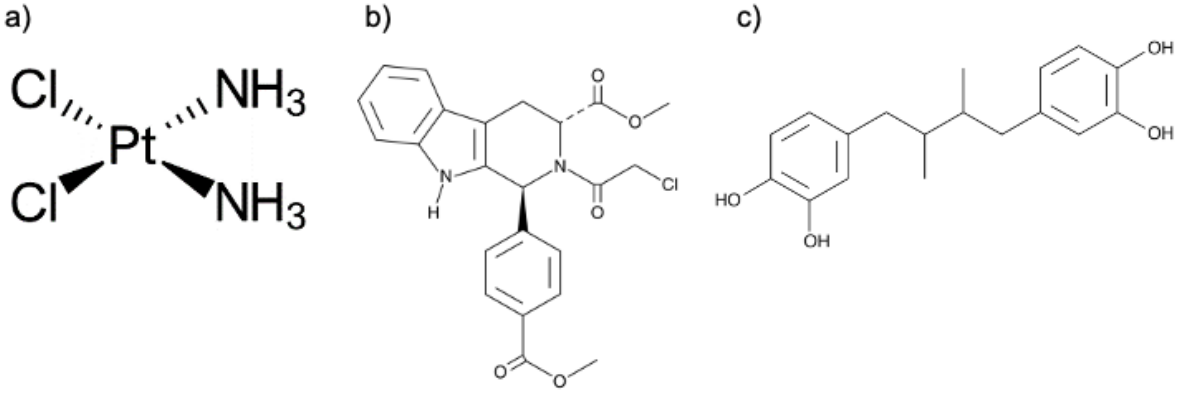

Figure 5: Structure of cisplatin (a) ferroptosis inducing agent (1S,3R)-RSL3[80] (b) and structure of LOX-inhibitor NDGA[81] (c)

The esterification of PUFAs into phosphatidylethanolamine (PE) via Acyl-CoA synthetase long-chain family member 4 (ACSL4) was identified as an essential step for ferroptosis. In breast cancer cell lines *Acsl4* expression directly correlates with their sensitivity to ferroptosis induction and *Acsl4 Gpx4* double knock out cells are viable demonstrating the essential role of ACSL4. Mechanistically, it catalyzes the esterification of CoA to fatty acids [82]. Those are then incorporated into PLs by Lysophosphatidylcholine acyltransferase (LPCAT)[83]. The exact structural effect of lipid ROS membrane incorporation is yet disputed, it is however thought to either cause a change in membrane curvature and membrane thinning leading to a perforation of the cell membrane or to cause the formation of structured pores as in pyroptosis[84]. Molecular dynamics simulations indicate, that an unrestricted incorporation of oxylipins into PLs might cause a feedback cycle of membrane oxidation that increases the curvature of a membrane thereby increasing the accessibility of the membrane for further oxidation leading to the decomposition of the membrane[73]. The phospholipid bilayer decomposition upon incorporation of oxidized PUFAs is illustrated in Figure 6.

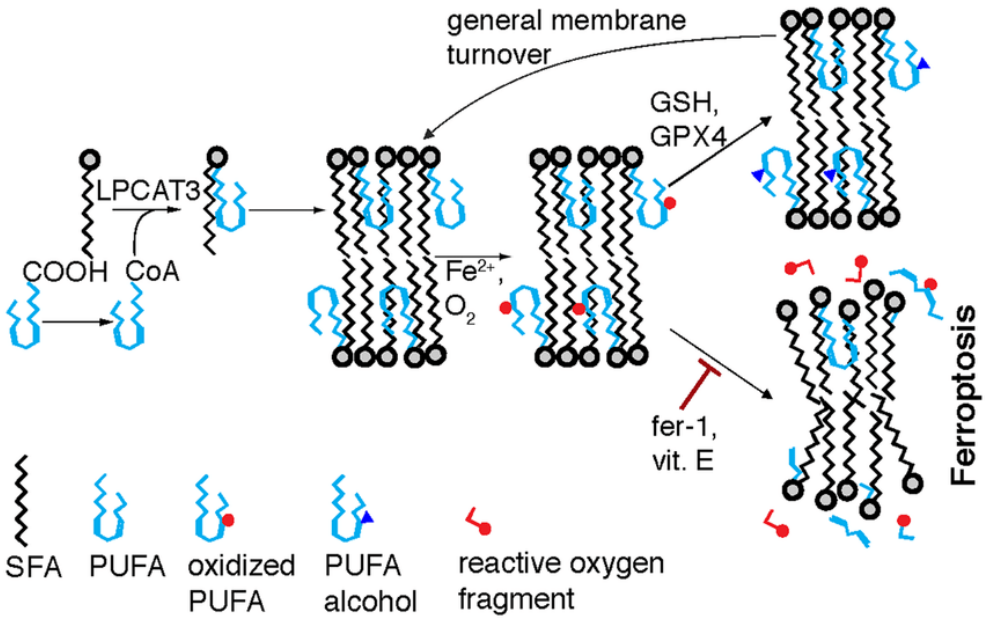

Figure 6: Disruption of phospholipid bilayer during ferroptosis through incorporation of oxidized poly unsaturated fatty acids (PUFAs). Lysophosphatidylcholine acyltransferase (LPCAT) incorporation of fatty acids into membrane, glutathione peroxidase 4 (GPX4) mediated reduction of peroxides with co-factor glutathione (GSH) and inhibition of ferroptosis via ferrostatin-1 (fer-1) or Vitamin E (vit. E) [73]

Ferroptosis provides an alternative way of RCD in cancer cells that are resistant to conventional chemotherapies, like the apoptosis-inducing cisplatin[85].

1.4 Extraction of fatty acids and oxylipins from human cells

Free atty acids and oxylipins are characterized in several types of biological samples such as blood plasma, tissue samples and cell culture medium[86]. Extracting esterified oxylipins from cell membranes by saponification provides the possibility to assess total fatty acid and oxylipin levels in biological samples[87]. Fatty acids and oxylipins act as auto- and paracrine mediators in numerous homeostatic functions and inflammation[86,88]. Abnormal signaling of oxylipins has a crucial role in cardiovascular diseases being linked to pathologies such as hypertension, diabetes, hemostasis and thrombosis[89]. For free oxylipins, robust solid phase extractions in combination with liquid chromatography mass spectrometry (SPE-LC-MS) methods have been established[86,88].

1.4.1 Saponification of esterified fatty acids and oxylipins

Biological membranes consist of phospholipid bilayers that emerge due to the amphiphilic properties of the phospholipids. In glycerophospholipids, these properties are caused by its two structural regions, a hydrophilic phosphate head group linked to two hydrophobic fatty acids via an ester bond to a glycerol. At sn-1 position, the glycerol is mostly bound to a saturated fatty acid, at sn-2 to an unsaturated fatty acid or an oxylipin and at sn-3 it is bound to a phosphate[90]. The general structure of a glycerophospholipid and its bilayer conformation are both illustrated in Figure 7.

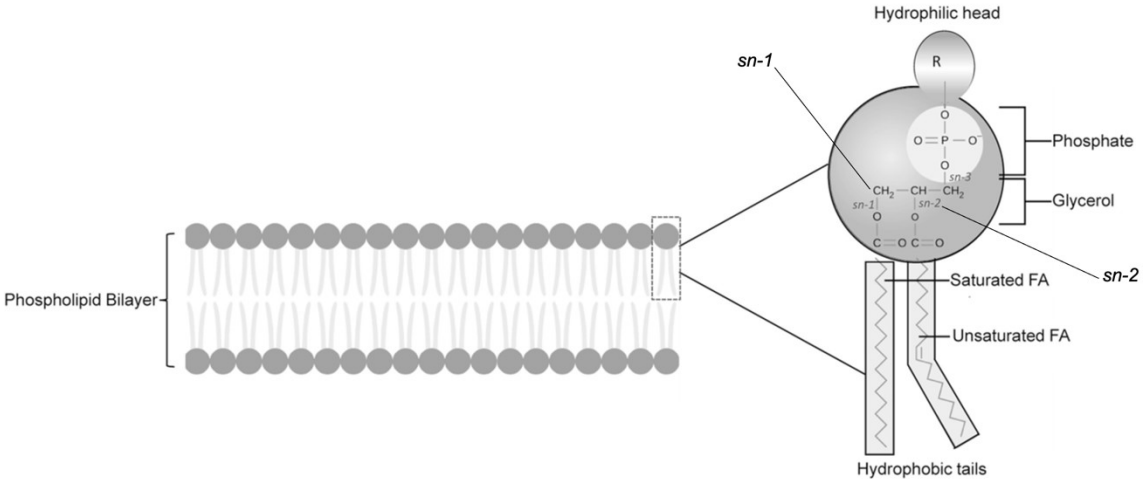

Figure 7: Structure of a glycerophospholipid and illustration of a phospholipid bilayer[18]

In order to identify and quantify fatty acids and oxylipin profiles from membranes, they have to be released from the glycerophospholipids. This can be achieved by chemical hydrolysis, *i.e.* saponification. During saponification, complex lipids are hydrolyzed by an alkaline solution to form fatty acid salts[91]. At least 56 oxylipins are stable during alkaline hydrolysis and can be quantitatively extracted by saponification, while some prostaglandins and leukotrienes undergo degradation with the exceptions of PGF_{2a} and LTB_4[84]. Especially prostaglandins with a β-hydroxy ketone system are prone to dehydration under acidic and basic conditions[87].

1.5 Sample preparation and instrumental setup for fatty acid analysis

1.5.1 Solid phase extraction

Solid phase extraction (SPE) is a sample preparation technique widely used to enrich analytes and reduce background matrix. During SPE, analytes in a liquid phase are extracted based on their interaction with a solid phase and significantly enriched accordingly. While analytes are retained at the solid phase the residual matrix is washed off. Subsequently, the purified analytes are eluted with a liquid phase that competes with the analyte to solid phase interactions or by thermal desorption into gas phase. Widely used solid phases are inorganic oxide adsorbents such as silica gel and polymeric solid phases such as poly(styrene-divinylbenzene)[92]. Currently, solid phase extraction (SPE) is the most commonly applied sample preparation method for oxylipins and PUFAs[93]. For the extraction of fatty acids and oxylipins during the course of this experiment, a poly(styrene-divinylbenzene) solid phase was used (Strata™-X 33 µm Polymeric Reversed Phase). After SPE of PUFAs and oxylipins, the analytes are usually completely dried under an inert gas such as N_2 and reconstituted in a fitting solvent for subsequent analysis or storage[94].

1.5.2 Reversed-phase ultra high-performance liquid chromatography

Reversed-phase ultra high-performance liquid chromatography (RP-UHPLC) in combination with electrospray ionization mass spectrometry (ESI-MS) is the most commonly used technique to analyze mixtures of PUFAs and oxylipins. The UHPLC technique is based on the interaction between a hydrophobic stationary phase and an analyte in a mobile phase[95]. In an RP-UHPLC setup, separation of lipid species occurs according to the lengths of alkyl chains and the number of double bonds that those possess[96]. The proper separation of oxylipin species is especially crucial due to the presence of numerous isobars in this compound class[97]. The separation of most oxylipin isobars can be achieved by using an UHPLC setup with a C18 column and a flow gradient[98]. To achieve the separation of enantiomeric oxylipins, the usage of chiral

columns emerged. Here the stationary phase is usually a derivative of cellulose or amylose. Due to the regiospecificity of oxygenases, the method is crucial for the distinction of non-enzymatically from enzymatically oxidized fatty acids[99]. In the course of this project, a reversed-phase separation method using a C18 column was chosen.

1.5.3 Mass spectrometry

Mass spectrometry has emerged as an indispensable detection method for the analysis of fatty acids and oxylipins[95]. The fundamental principle of mass spectrometry is the ionization of analytes and separation of those ions according to their mass-to-charge (m/z) ratio. Tandem mass spectrometry is a technique that involves the isolation of an ion of a certain m/z ratio, its fragmentation and subsequent measurement of the produced fragments[100]. Tandem mass spectrometry thereby enables the distinction of isomers which is essential for the identification of oxylipins. Such analyses can be performed either with targeted or untargeted approaches. If the goal is to investigate specific analytes, a targeted approach can be implemented. One of the most common methods for targeted analysis is multiple reaction monitoring, in which a triple quadrupole is used to isolate a specific precursor ion, fragment it and identify predefined fragments[101]. To discover all detectable analytes in samples and to identify a large number of analytes in one single run, untargeted approaches are required. These approaches require high resolution MS such as an orbitrap to discriminate between isobaric species and are usually coupled to an UHPLC setup[101]. In order to identify analytes in such setups, it is essential to establish a standard compound database that provides information about retention times during UHPLC and fragmentation patterns that emerge in a certain device. Furthermore, internal deuterated standards can be introduced to enable the correction of retention time shifts and to account for the sample preparation quality. In addition, online databases such as the LIPIDMAPS open-source data base provide MS2 spectra of lipid species that can be crucial for the identification of analytes[95]. During this project, an untargeted approach was chosen using an Agilent Infinity 1290 UHPLC system equipped with a reversed-phase column coupled to an orbitrap Exploris 480.

2. Research justification

The analysis of fatty acids and oxylipins in biological samples provides important insight (patho-)physiological processes, especially related to inflammation signalling, differentiation and others. Bioactive oxylipins are enzymatically released from membranes, subsequently oxidized and secreted. Consequently, these low abundant signalling molecules are often analysed by LC-MS/MS in blood plasma or cell supernatants, after a solid-phase enrichment. Interestingly, only 18% of oxylipin publications since 2020 investigated membrane-bound fatty acids and oxylipins[102]. These are usually assessed by lipidomic profiling of complex lipids, such as glycerophospholipids, diglycerides and triglycerides, amongst others. The aim of this master thesis was to implement and optimize a saponification-based extraction method to profile membrane-bound fatty acids and oxylipins as a complementary technique to the analysis of their free counterparts. This enables to characterize an under-investigated aspect of differentiation and cell death mechanisms *in vitro*, including apoptosis and ferroptosis. As a secondary aim, the fatty acid and oxylipin profiles of whole cell lysates will be compared to that of an enriched mitochondrial fraction in a cell death model *in vitro*.

3. Materials and Methods

3.1 Materials

Table 1:Chemical list with used abbreviations and producers

Chemical	**Abbreviation**	**Producer**
Acetonitrile	ACN	Fisher Chemical
(1S,3R)-RSL3	RSL3	Sigma-Aldrich
3-(4,5-dimethylthiazol-2-yl)-2,5-diphenyltetrazolium bromide (98%)	MTT	Acros Organics
Cisplatin	CisPt	Sigma-Aldrich
Dimethyl Sulfoxide	DMSO	Sigma-Aldrich
Ethanol (99.8%)	EtOH (99.8%)	Fisher Chemical
Ethanol (99.9%)	EtOH (99.9%)	AustrAlco
Fetal bovine serum	FBS	Biowest
Formic acid	FA	Sigma-Aldrich
Glycine	Gly	Merck
Hydrochloric acid (37%)	HCl	Merck
Methanol	MeOH	VWR International
Nordihydroguaiaretic acid	NDGA	Cayman Chemical
Penicillin-Streptomycin		Sigma-Aldrich
Phosphate-buffered saline	PBS	Sigma-Aldrich
Potassium hydroxide	KOH	Sigma-Aldrich
RPMI-1640		Sigma-Aldrich
Trypsin-Ethylenediaminetetraacedic acid	Trypsin-EDTA	Gibco

3.2 Cell culture

The promyeoloblast cell line HL-60 and the ovarian carcinoma cell line A2780 were used for this project. For both, HL-60 and A2780, incubation was performed at 37°C and 5% CO_2 in a humidified atmosphere incubator (Heracell 150i CO2 Incubator, Thermo Scientific). RPMI-1640-medium, supplemented with 10 % fetal bovine serum and 1% penicillin-streptomycin, was used for both cell lines. Cells were counted using a 0.100 mm Neubauer plate (Marienfeld) and a Cell Drop Bright Field Cell Counter (DeNovix). The cells were handled under a sterile environment in the Herasafe KS 12 microbiological safety cabinet (ThermoScientific).

3.2.1 Promyeoloblast cell line HL60

The promyeoloblast cell line HL-60 (kindly provided by M. Jakupec, Faculty of Chemistry, University of Vienna, Austria) was used as a model system for myeoloid differentiation. The cells were cultivated in 75 cm² culture flasks (T75 for suspension cells with filter cap; Sarstedt). The medium was changed every 2 to 3 days and the cells split to maintain a concentration of 10^5 to 10^6 cells ml^{-1}.

3.2.2 Ovarian carcinoma cell line A2780

The ovarian carcinoma cell line A2780, kindly provided by Thomas Grunt (Medicinal University of Vienna, Austria), was used as a model system for apoptosis and ferroptosis. The cells were cultivated in 75 cm² culture flasks (T75 for adherent cells with filter cap; Sarstedt). At a confluence of about 80% the cells were splitted: Cell medium was removed, the cells were washed with 3.5 mL sterile PBS and then incubated in 3 mL trypsin-EDTA-solution for 10 min. Then, 7 mL medium was added and residual adherent cells detached from the culture flask by pipetting. The cells were then pelleted at 1100 rpm (Heraeus Megafuge 16R; Thermo Scientific™) for 5 min and resuspended in 1 mL cell medium. Subsequently, the cells were split at a ratio between 1:3 and 1:6.

3.3 Cell viability and synergy assays

Cell viability and synergy testing of combination treatments were conducted using A2780 cells on 96 well plates (Sarstedt). Each well was seeded with 100 µL of a 10^4 cells well^{-1} suspension in medium and incubated for 24 h. Each row included an additional well for untreated control cells and a well for a medium blank. All compound solutions were prepared from stock solutions in DMSO, diluted with cell medium. 24 h post seeding, inhibitiors were added in 100 µL complete medium containing 2× compound concentrations for viability assays and 4× compound concentrations for the synergism assay, the control cells and medium blank were supplemented with 100 µL complete medium resulting in wells containing 200 µL medium each with the appropriate treatment concentration. Following a 24 h incubation period, 20 µL of a solution of MTT (5 mg ml^{-1} PBS) was added to each well. Subsequently, the cells were incubated for further 3h. Then, the supernatant was removed and the remaining formazan crystals were dissolved in DMSO. Once the formazan crystals were completely dissolved, the absorbance at 570 nm of each well was measured using an UV/Vis spectrophotometer (Multiskan Go, Thermo Fisher Scientific). Viability was calculated according to Equation 1.

$$Viability_{\%} = \frac{absorbance_{sample} - average\ absorbance_{blank}}{average\ absorbance_{control} - average\ absorbance_{blank}} \times 100$$

Equation 1: Medium blank corrected viability percentage calculated from absorbance

3.3.1 Cell viability assays

The viability of A2780 cells in the presence of different concentrations of RSL3 and NDGA was investigated. Each assay was performed in independent triplicates using at least technical triplicates, with 8 inhibition concentrations, cell blanks and medium blanks. NDGA was dissolved in DMSO to obtain a 100 mM stock solution. For each assay, a new stock solution was produced. This stock solution was then diluted with

cell medium to obtain a 240 µM and a 160 µM solution that were further diluted in series to obtain the concentrations of the 2X solutions with their respective treatment concentrations depicted in Table 2. RSL3 was obtained from a 10 mM solution in DMSO stored at -20°C. The RSL3 solution was diluted in medium to an 800 nM solution which was then used to individually prepare each inhibition solution by further dilution with cell medium. The treatment concentrations are depicted in **Fehler! Verweisquelle konnte nicht gefunden werden.**. GraphPad Prism 6 (Dotmatics) was used to plot inhibition curves (Log_{10} of inhibition concentrations vs normalized inhibition) and to compute the IC_{50} values by a nonlinear regression model with four parameters with a variable slope.

Table 2: NDGA and RSL3 concentrations for viability assays

NDGA [µM]	120	80	60	40	30	20	10	5
RSL3 [nM]	125	110	95	80	65	50	35	20

3.3.2 Synergy assay

A synergy assay was performed by the combination of NDGA and RSL3 in A2780 cells. On a 96 well plate, an 8 × 8 matrix featuring increasing NDGA and RSL3 concentrations summarized in Table 3 was prepared. Further, 8 wells each for untreated cells and medium blank were seeded. A synergism matrix was then computed using the webtool SynergyFinder 3.0 employing the Bliss/Loewe consensus method [103].

Table 3: Concentrations of RSL3 and NDGA of treatment matrix on A2780

NDGA	RSL3								
		IC 0	**IC 10**	**IC 25**	**IC 40**	**IC 50**	**IC 60**	**IC 75**	**IC 90**
		0 nM	31 nM	38 nM	42 nM	45 nM	49 nM	55 nM	60 nM
	IC 0	RSL3 0nM	RSL3 31nM	RSL3 38nM	RSL3 42nM	RSL3 45nM	RSL3 49nM	RSL3 55nM	RSL3 60nM
	0µM	NDGA 0µM	NDGA 0µM	NDGA 0µM	NDGA 0µM	NDGA 0µM	NDGA 0µM	NDGA 0µM	NDGA 0µM
	IC 10	RSL3 0nM	RSL3 31nM	RSL3 38nM	RSL3 42nM	RSL3 45nM	RSL3 49nM	RSL3 55nM	RSL3 60nM
	4 µM	NDGA 4µM	NDGA 4µM	NDGA 4µM	NDGA 4µM	NDGA 4µM	NDGA 4µM	NDGA 4µM	NDGA 4µM
	IC 25	RSL3 0nM	RSL3 31nM	RSL3 38nM	RSL3 42nM	RSL3 45nM	RSL3 49nM	RSL3 55nM	RSL3 60nM
	10 µM	NDGA 10µM	NDGA 10µM	NDGA 10µM	NDGA 10µM	NDGA 10µM	NDGA 10µM	NDGA 10µM	NDGA 10µM
	IC 40	RSL3 0nM	RSL3 31nM	RSL3 38nM	RSL3 42nM	RSL3 45nM	RSL3 49nM	RSL3 55nM	RSL3 60nM
	19 µM	NDGA 19µM	NDGA 19µM	NDGA 19µM	NDGA 19µM	NDGA 19µM	NDGA 19µM	NDGA 19µM	NDGA 19µM
	IC 50	RSL3 0nM	RSL3 31nM	RSL3 38nM	RSL3 42nM	RSL3 45nM	RSL3 49nM	RSL3 55nM	RSL3 60nM
	26 µM	NDGA 26µM	NDGA 26µM	NDGA 26µM	NDGA 26µM	NDGA 26µM	NDGA 26µM	NDGA 26µM	NDGA 26µM
	IC 60	RSL3 0nM	RSL3 31nM	RSL3 38nM	RSL3 42nM	RSL3 45nM	RSL3 49nM	RSL3 55nM	RSL3 60nM
	39 µM	NDGA 39µM	NDGA 39µM	NDGA 39µM	NDGA 39µM	NDGA 39µM	NDGA 39µM	NDGA 39µM	NDGA 39µM
	IC 75	RSL3 0nM	RSL3 31nM	RSL3 38nM	RSL3 42nM	RSL3 45nM	RSL3 49nM	RSL3 55nM	RSL3 60nM
	72 µM	NDGA 72µM	NDGA 72µM	NDGA 72µM	NDGA 72µM	NDGA 72µM	NDGA 72µM	NDGA 72µM	NDGA 72µM
	IC 90	RSL3 0nM	RSL3 31nM	RSL3 38nM	RSL3 42nM	RSL3 45nM	RSL3 49nM	RSL3 55nM	RSL3 60nM
	195 µM	NDGA 195 µM	NDGA 195 µM	NDGA 195 µM	NDGA 195 µM	NDGA 195 µM	NDGA 195 µM	NDGA 195 µM	NDGA 195 µM

3.4 Cell culture, preparation and treatments for total oxylipin extraction

The total oxylipin extraction was performed with A2780 and HL60 cells seeded onto 6 well plates (Sarstedt). For each cell line, 2 mL cell suspension was seeded and incubated at 37°C and 5% CO_2 in a humidified atmosphere (Heracell 150i CO2 Incubator; Thermo Scientific).

3.4.1 Induction of apoptosis and ferroptosis in A2780

The first model, that was studied by the extraction of all oxylipins in cell samples were A2780 cells undergoing ferroptosis and apoptosis. The investigation of the total oxylipin

fraction of apoptotic and ferroptotic A2780 cells was performed in 2 iterations to optimize the saponification method (20 min saponification incubation with 10^5 cells well^{-1}), adjust the concentration of the ferroptosis inducing agent RSL3 and investigate an additional state of NDGA induced ferroptosis inhibition. The treatment concentrations, seeded cell numbers and saponification conditions are detailed in Table 4 and Table 5. All treatments were carried out 24 h after seeding and included an incubation time of 24 h. Of each treatment, 4 replicates and additionally 4 untreated vehicle controls (0.0044% DMSO) were prepared. To account for DMSO effects, the final DMSO concentration of each sample was equalized to 0.0044%.

Table 4: Treatment concentrations of A2780 cell systems investigated by total oxylipin extraction at initial method conditions (30 min saponification, 2×10^5 cells well^{-1})

Samples for preliminary saponification		
Cells well	200000	
Saponification [min]	30	
	RSL3 [nM]	CisPt [µM]
Ferroptosis	106	-
Apoptosis	-	9
Control	-	-

Table 5: Treatment concentrations of A2780 cell systems investigated by total oxylipin extraction at optimized method conditions (20 min saponification, 1×10^5 cells well^{-1})

Samples for optimized saponification conditions			
Cells well	100000		
Saponification [min]	20		
	RSL3 [nM]	NDGA [µM]	CisPt [µM]
Ferroptosis	38	-	-
Inhibited ferroptosis	38	4	-
Apoptosis	-	-	9
Control	-	-	-

3.4.2 Mitochondrial fraction of apoptotic and ferroptotic A2780

To investigate the profiles of oxylipins in the mitochondrial fraction of A2780 cells after different treatments, a sequential centrifugation approach to extract a crude mitochondrial fraction was performed. A2780 cells suspended in medium (10 ml, $5*10^5$ cells ml^{-1}) were seeded into T75 flasks and incubated for 24 h. Then, the medium in each culture flask was removed, 10 mL medium spiked with the respective treatment (38 nM RSL3, 9 µM Cisplatin, control without added compound) were added onto each culture and the cells incubated for 24h. Subsequently, the medium was removed, the cells washed with 3 mL PBS and trypsinized with 3 mL trypsin-EDTA-solution for 10 min at 37°C and 5% CO_2. The cells were then transferred into 10 mL falcon tubes and centrifuged at 1100 RPM for 5 min at 4°C (Heraeus Megafuge 16R; Thermo Scientific™), the supernatant discarded. The cells were then washed twice by resuspension in 2 mL PBS and centrifugation at 1100 RPM for 5 min at 4°C (Heraeus Megafuge 16R; Thermo Scientific™). To the washed cell pellet, 2 mL of an isotonic buffer solution was added (10 mM HEPES (pH 7.4), 10 mM NaCl, 250 mM Sucrose, 3.5 mM MgCl2, 1 mM EGTA, 0.5% Triton X-100, PMSF 1mM, PPC 1%). Then, the cells in buffer were frozen in liquid N_2 and rapidly thawed in a water-bath at 37°C. Subsequently, the cell solution was pressed through a 23-gauge needle 5 times and the solution centrifuged at 3’500 rpm at 4°C for 5 min (Centrifuge 5424; Eppendorf™) and the supernatant was transferred into 2 mL Eppendorf tubes, which was centrifuged at 15000 g at 4 °C for 5 min.The supernatant was discarded, the mitochondria-containing pellet resuspended in 1 mL PBS and again centrifuged at 15000 g at 4°C for 5 min (Centrifuge 5424; Eppendorf™). The resulting mitochondrial pellet was then worked up according to the total oxylipin extraction protocol by directly adding the saponification mix into the Eppendorf, incubation was performed for 20 min.

3.4.3 Differentiation of HL-60 cells

HL-60 cells were seeded onto a 6-well plate at a concentration of 10^5 cells ml^{-1} in 2 mL medium, treated with 1.25% DMSO per well to initiate differentiation, and incubated for 48 h. Then, 1 µL TGF-β1 (1 µg ml^{-1}) was added and the cells were incubated for 24 h. To harvest both, suspended and adherent cells, the medium with the suspended cells was centrifuged at 1100 RPM, the adherent cells were washed and then processed by saponification.

In a similar setting, HL-60 cells were treated with ATRA (1µM) per well to initiate differentiation and incubated for 72h. Then, the treatment was increased to 6µM ATRA and 3 replicates were additionally treated with 1 µL TGF- β1 (1 µg ml^{-1}) incubated for 48 h, washed and then processed by saponification.

3.5 Total fatty acid and oxylipin extraction of cell samples

To determine the total levels of fatty acids and oxylipins including esterified from cellular samples, KOH mediated saponification was performed[87]. In this study, an existing general approach was adjusted the available lab conditions and tested on different biological systems (HL60 and A2780, cells in suspension and adherent cultures respectively). Further, the method was then optimized for the treatment of adherent cells in the form of the cell line A2780. Finally, the saponification method was then tested for mitochondrial fractions.

To purify the samples, a solid phase extraction (SPE) was performed, all samples were then measured in an HPLC-MS setup. For identification and validation of the method, 2 internal standard mixtures were added to each sample, one (eicosanoid mix pre) prior to the SPE and another (eicosanoid mix post) immediately prior to the HPLC-MS measurement. The contents of the standard mixtures are summarized in Table 6 and Table 7. All standards were purchased from Cayman Chemicals, diluted in ACN and stored at -80°C.

Table 6 Internal standards – "eicosanoid standards pre" concentrations and abbreviations

Internal standards - eicosanoid standards pre	Abbreviation	c [pg μL^{-1}]
12S-hydroxyeicosatetraenoic acid-d8	12S-HETE-d8	6,67
15S-hydroxyeicosatetraenoic acid-d8	15S-HETE-d8	6,67
5-oxo-eicosatetraenoic acid-d7	5-OxoETE-d7	20,00
11,12-dihydroxy-5Z,8Z,14Z-eicosatrienoic acid-d11	11,12-DiHETrE-d11	6,67
prostaglandin E-d4	PGE-d4	13,33
20-hydroxyeicosatetraenoic acid-d6	20-HETE-d6	6,67

Table 7 Internal standards – "eicosanoid standards post" concentrations and abbreviations

Internal standards - eicosanoid standards pre	Abbreviation	c [pg μL^{-1}]
5S-hydroxyeicosatetraenoic acid-d8	5S-HETE-d8	6,67
14,15-dihydroxy-5Z,8Z,14Z-eicosatrienoic acid-d11	14,15-DiHETrE-d11	6,67
8-iso Prostaglandin F2alpha-d4	8-iso-PGF2alpha-d4	13,33

3.5.1 Saponification mediated total oxylipin extraction

To extract esterified oxylipins from cell samples, a potassium hydroxide mediated saponification was performed. Cell samples and all reagents were placed on ice throughout the process. First, medium was removed and the cells washed with 1 mL of phosphate buffered saline (PBS, Sigma-Aldrich). Then a solution of 25 µL potassium hydroxide (KOH, 4M, Sigma-Aldrich) and 225 µL ethanol (EtOH, 99.8%; Fisher Chemical) was added onto each well followed by an incubation at 37°C and 5% CO_2 in a humidified atmosphere (Heracell 150i CO2 Incubator; Thermo Scientific). Subsequently, 1.75 mL of a glycine-HCl buffer (0.1 mM, pH 4) was added. The cell lysates were then quantitatively transferred into falcon tubes (Polypropylene) and 8 mL of ethanol (99.9%, -20°C) was added. Before storing the samples for at least 24 h at -20°C, they were spiked with an eicosanoid standard mix (eicosanoid standards pre). The saponification is illustrated in Figure 8.

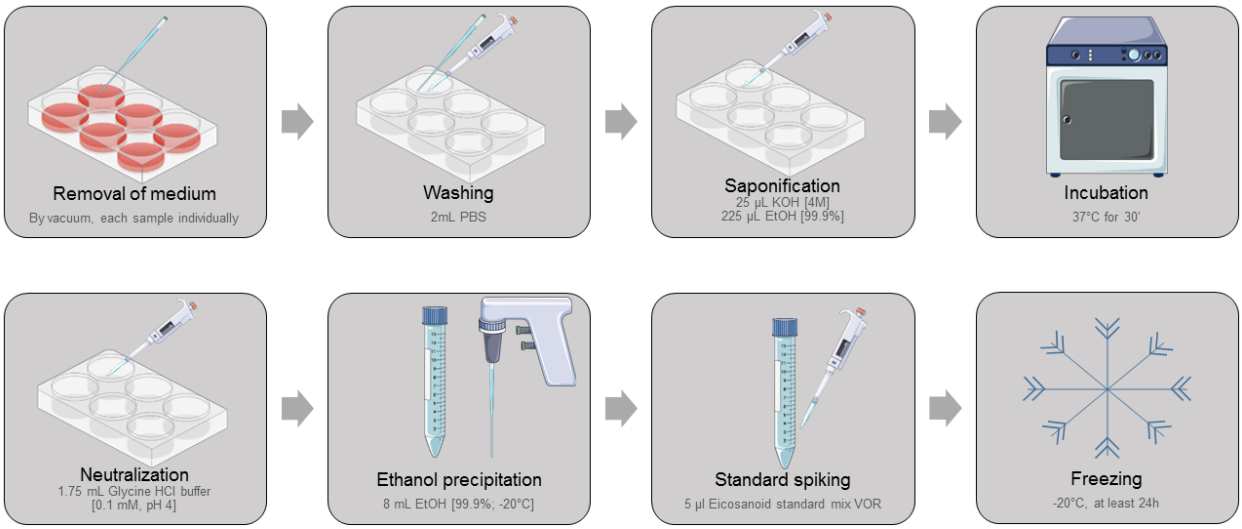

Figure 8: Steps of saponification of adherent cell samples with the key properties of each step with illustrations. It was partly generated using Servier Medical Art, provided by Servier, licensed under a Creative Commons Attribution 3.0 unported license.

Due to the fact, that the HL-60 cells were partially only adherent, the protcol was adapted for the processing of their samples. To harvest both, suspended and adherent

cells, the medium with the suspended cells was centrifuged at 1100 RPM. The adherent cells were treated with a solution of 25 µL potassium hydroxide (KOH, 4M, Sigma-Aldrich) and 225 µL Ethanol (EtOH, 99.8%; Fisher Chemical) for 10 min and then added to the pellet of the suspended cells into a falcon tube. The cells in the KOH EtOH solution were then incubated at 37°C in a water bath for 30 min. The neutralization was then performed by adding 1.75 mL of a glycine-HCl buffer (0.1 mM, pH 4, 4°C) into the falcon tubes placed on ice. Precipitation, standard spiking and storage was performed analogously to the standard saponification mediated total oxylipin extraction.

3.5.2 Optimization of sample preparation and properties of total oxylipin extraction

To optimize the method of total oxylipin extraction in the cell line A2780 by KOH mediated saponification, the influence of cell density and duration of saponification on the results were investigated. The impact of saponification duration was investigated at a cell density of 10^5 cells well^{-1} and the influence of cell density was evaluated with a 30 min. The 2 parameters were investigated separately and are summarized in **Fehler! Verweisquelle konnte nicht gefunden werden.**.

Table 8.: Sample preparation for the saponification-optimization. On top, the different A2780 cell numbers of a 30 min saponification are summarized. On the bottom, the different incubation times of saponification are depicted for wells with 1×10^5 cells well^{-1}.

30 min	Cells well^{-1}	200000	100000	50000	25000
100000 cells	Saponification [min]		30	20	10

3.5.3 Solid phase extraction

After EtOH precipitation, the samples were centrifuged for 30 min (5000 rpm, 4°C, Megafuge 16R**,** Thermo Scientific™), the supernatant collected and its ethanol content evaporated in a vacuum concentrator (Genevac™, Thermo Scientific™). Subsequently, solid phase extraction was performed by loading the samples onto

StrataX SPE columns (30 mg mL^{-1}; Phenomenex). Prior to the extraction, the columns were washed 2 times with 1 mL MeOH (4°C, MS-grade) and then equilibrated with 2 times 1 mL H_2O (4°C, MS-grade). The samples were then loaded onto the columns using Pasteur pipettes, washed with 2 times with 2 mL water (4°C, MS-grade) and eluted with 500 µL elution solvent (MeOH + 2% formic acid, +4°C). Under a nitrogen stream, the MeOH was then evaporated, the dried samples were dissolved in a reconstitution solvent (H_2O:ACN:MeOH + 0.2 % FA–vol% 65:31.5:3.5), spiked with 5 µL eicosanoid standard mixture post and immediately measured by LC-MS.

3.5.4 LC-MS analysis

The LC-MS setup to separate and measure the analytes consisted of an Agilent 1290 Infinity II UHPLC system (Agilent Technologies, Austria) equipped with a Phenomenex™ Kinetex™ XB-C18 column (150 x 2.1 mm; 2.6 µm) coupled to an Orbitrap Exploris™ 480 mass spectrometer (Thermo Scientific™) with a heated electrospray ionization source (EASY-IC™, Thermo Scientific™). A gradient elution chromatography with a mobile phase A consisting of H_2O + 0.2% FA and a mobile phase B consisting of ACN:MeOH (vol% 90:10) was performed with a flow rate of 200 µL min^{-1} at 40°C. Starting conditions were 35% B for 30 sec, which was then increased to 90% (1-10min) and subsequently further increased to 99% in 30 sec and maintained for 5 min. The HESI was operated in negative mode and set to the scan-to-scan mode applied for internal mass calibration with a range of 250-450 m/z and 250-700 m/z. Fragmentation was performed by higher-energy collisional dissociation (24% normalized collision energy), the spray voltage was set to 3.5 kV. The capillary temperature was set to 300°C and the temperature of the source to 380°C.

4. Results and discussion

4.1 Viability assays of ferroptosis inducer and inhibitor in A2780

To investigate the involvement of oxylipin mediation in ferroptosis, viability assays of the ferroptosis inducing agent RSL3 and of the ferroptosis inhibitor NDGA were performed. Subsequently, a synergism assay with RSL3 and NDGA was performed to determine the treatment conditions with the highest NDGA induced recovery in ferroptotic A2780 cells.

4.1.1 Cell viability of A2780 cells under RSL3 and NDGA treatment

All viability assays were performed in independent triplicates, the results are illustrated in viability curves in Figure 9. Prominently, a difference in the shapes of the dose-response curves can be noted. The RSL3 treatment resulted in a sigmoidal dose-response which indicates a concentration threshold for the efficacy of this treatment. This is characteristic for cytotoxic agents with specific molecular targets[104]. The decay-like dose response of NDGA on the contrary suggests that cytotoxicity is more likely the result of an increasing incapability to balance the antioxidant effects of NDGA. The IC_{50} value was computed by a sigmoidal fit model with GraphPad Prism 6 (Dotmatics) and 95% confidence intervals. The IC_{50} of NDGA in the ovarian cancer cell line A2780 is 45.72 ± 0.51 µM. This viability roughly corresponds to a study that investigated the viability of the human breast cancer cell line SKBR3 (IC_{50} = 31.09 ± 1.6 µM) and the human melanoma cell line MDA-MB-435 (IC_{50} = 38.8 ± 2.1 µM)[105]. The IC_{50} of RSL3 in the ovarian cancer cell line A2780 is 45.5 ± 1.1 nM. When compared to the human colorectal cancer lines HCT116 (IC_{50} = 4.1 µM), LoVo (IC_{50} = 2.8 µM), and HT29 (IC_{50} = 12 µM), the IC_{50} of RSL3 in A2780 cells remarkably turned out to be at least 2 orders of magnitude lower[106].

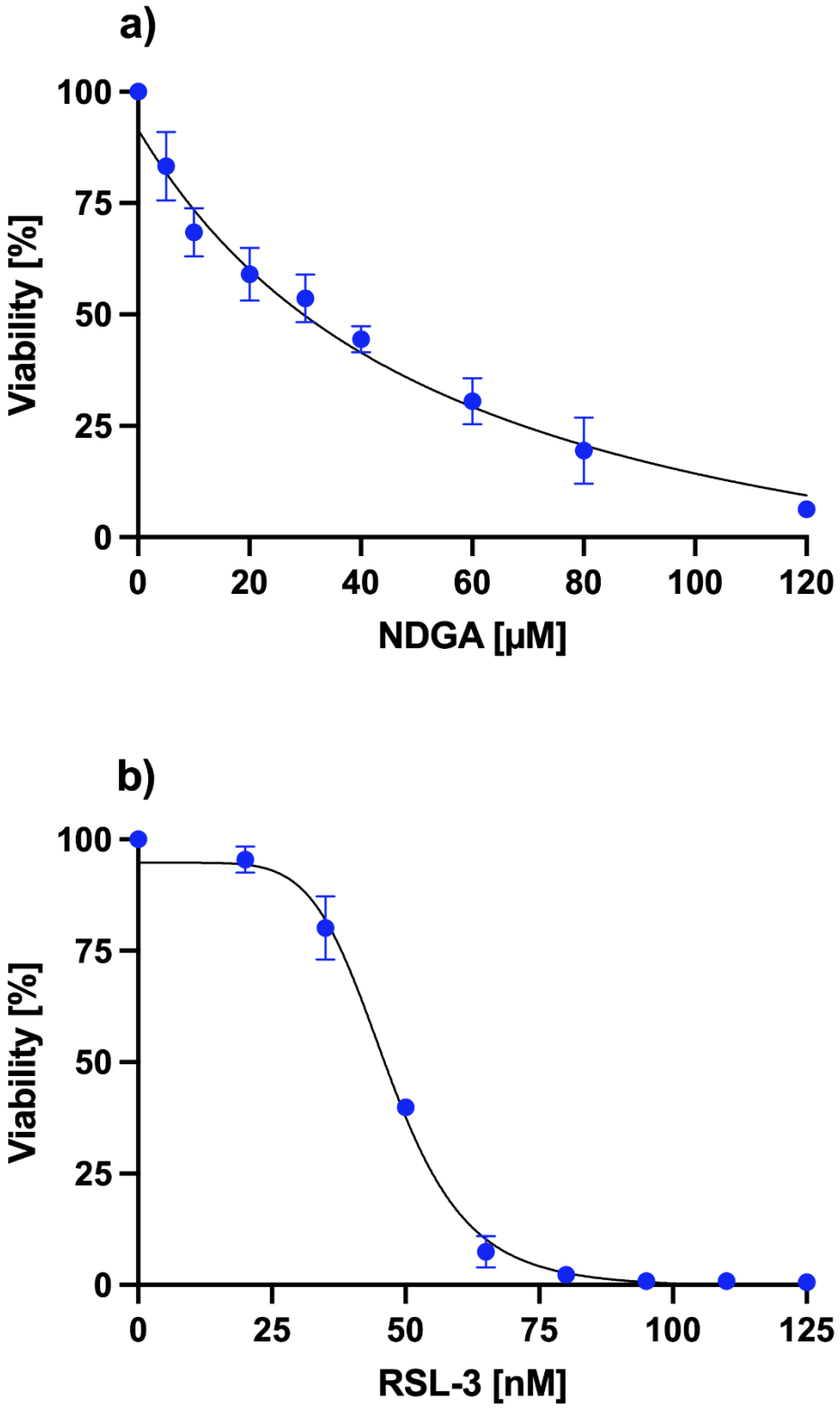

Figure 9: Viability curves of A2780 cells at a) NDGA treatment and b) RSL3 treatment

4.1.2 Synergism of RSL3 and NDGA in A2780 cells

Subsequently, the findings of the viability assays were then used to estimate the IC-values that were treated in a synergism assay between NDGA and RSL3 in A2780 cells in a 24 h incubation. The viabilites are summarized in Table *9*.

Table 9: Viabilites of A2780 in RSL3 and NDGA co-treatment titration after 24 h incubation.

RSL3 [nM]									
	60	11,4%	88,3%	60,6%	46,6%	32,8%	1,9%	6,3%	5,1%
	55	13,5%	81,0%	51,9%	47,7%	19,6%	12,3%	2,4%	8,8%
	49	18,6%	69,9%	57,2%	36,3%	36,2%	9,0%	7,8%	4,3%
	45	27,0%	82,6%	64,2%	35,1%	30,9%	2,9%	3,7%	5,1%
	42	28,7%	72,8%	54,8%	41,2%	38,9%	2,2%	3,4%	5,0%
	38	57,7%	84,2%	60,2%	49,2%	33,9%	3,1%	2,8%	10,1%
	31	77,6%	91,5%	73,5%	55,0%	35,3%	4,0%	7,1%	5,2%
	0	108,1%	86,2%	64,7%	53,3%	36,6%	1,9%	6,7%	8,9%
A2780		**0**	**4**	**10**	**19**	**26**	**39**	**72**	**195**
		NDGA [µM]							

A synergism matrix computed using the webtool SynergyFinder 3.0 employing the Bliss/Loewe consensus method[103] is illustrated in Figure 10. Strong antagonistic effects were especially observed in all RSL3 treatments, that received a 4 µM and 10 µM NDGA co-treatment.

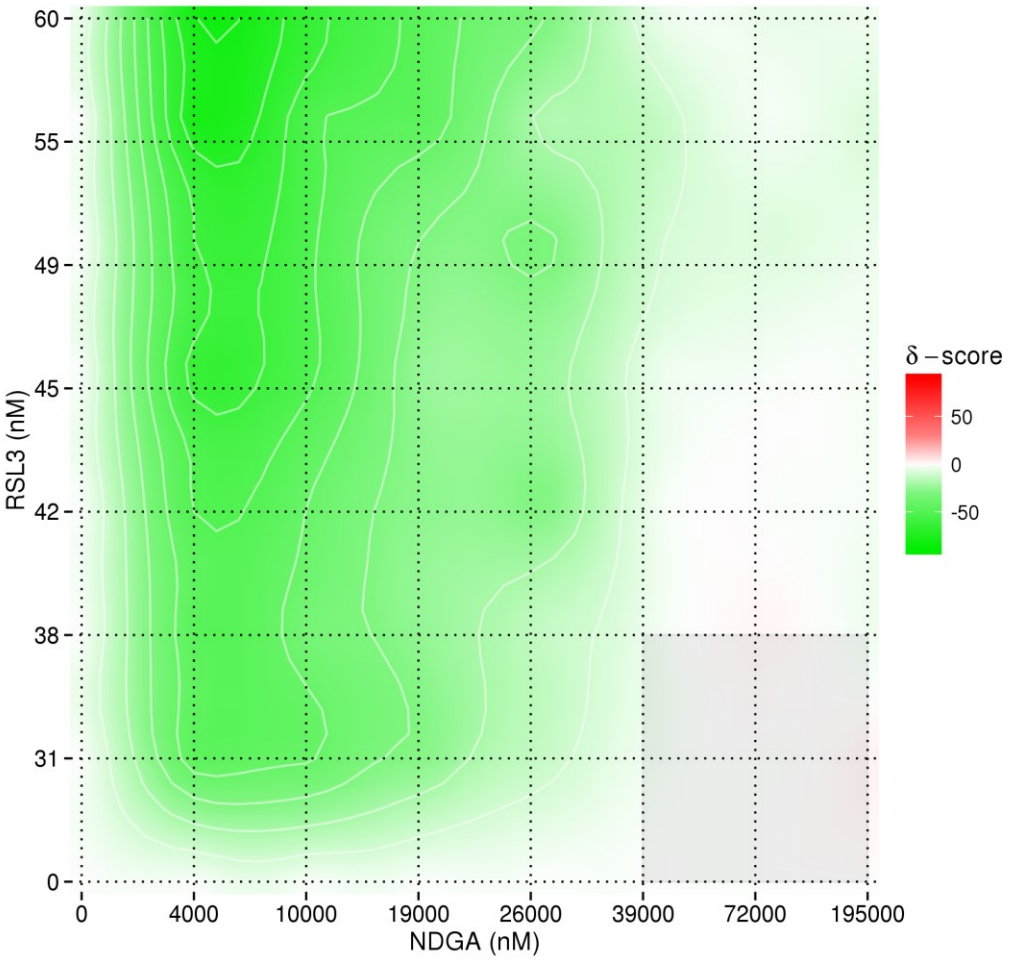

Figure 10: Bliss-Loewe synergy matrix of NDGA and RSL3 depicting antagonistic effects in a green color-scheme.

Overall, it can be concluded, that an NDGA treatment can decrease the sensitivity of A2780 cells to RSL3. As a 5-LOX inhibitor, NDGA prevents the oxidation of PUFAs. It thereby decreases the stress on the cell, that occurs during GPX-4 inhibition mediated accumulation of oxylipins[72]. The highest cell recovery took place at the lowest investigated NDGA concentration (4 µM).

4.2 Optimization of the saponification mediated oxylipin extraction

To optimize the sample preparation protocol and extraction of esterified fatty acids and oxylipins in adherent A2780 cells, untreated cell samples were prepared. The concentration of cells per sample and the length of the saponification step were subject of investigation. In total, 85 analytes were investigated, the coefficients of variation (CVs) of each analyte computed, and used to compare each method. Each analyte was normalized with the *eicosanoid standards pre* that are summarized in Table *6*. The results are illustrated in Figure 11.

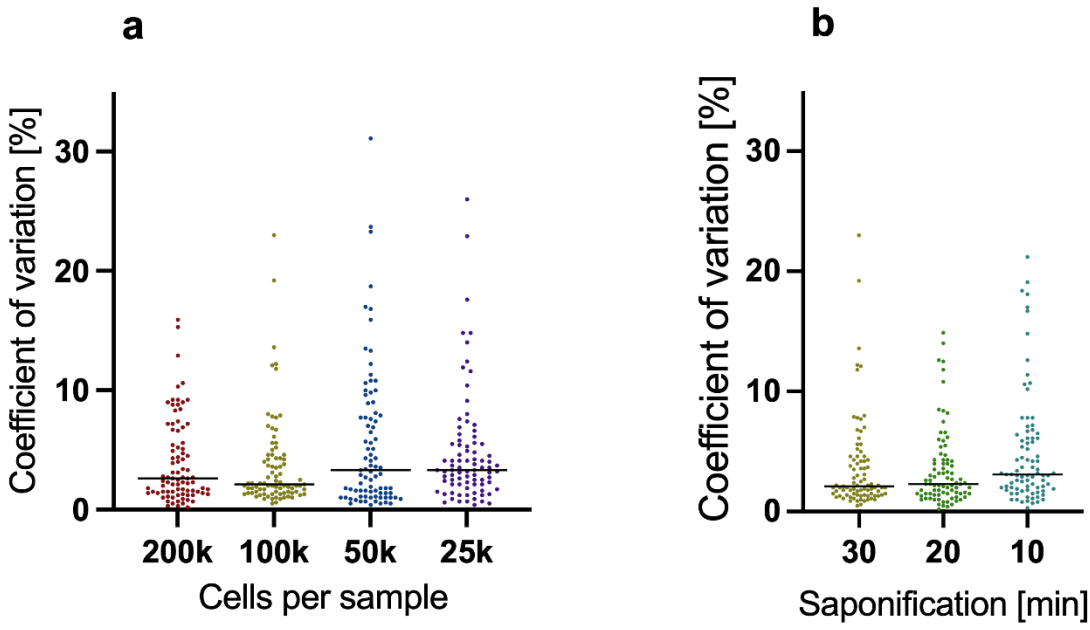

Figure 11: CVs of normalized analytes and median CV of different oxylipin extraction conditions. In a) varied cell densities per sample with a 30-minute saponification are depicted. In b) varied lengths of saponification with samples of 10^5 cells per sample are illustrated.

In total, 73 analytes were identified. The median CVs of the normalized analytes were between 2.1% and 3.3% in each sample. Samples with at least 10^5 cells per sample and a saponification period of at least 20 minutes showed about 0.7% to 1.2% lower median CVs compared to those with $5*10^4$ and $2{,}5*10^4$ cells per sample or a saponification period of 10 min. Each median CV is summarized in Table *10*.

Table 10: Median CVs in different oxylipin extraction conditions

30 min saponification				100.000 cells		
200k	100k	50k	25k	30min	20min	10min
2,6%	2,1%	3,3%	3,3%	2,1%	2,3%	3,1%

To assess the quality of the sample preparation in each method condition, the CVs of the 9 deuterated standards summarized in Table *6* and Table *7* were assessed and are illustrated in Figure 12. It must be noted, that the data used to investigate the standards are not normalized in contrast to the analytes.

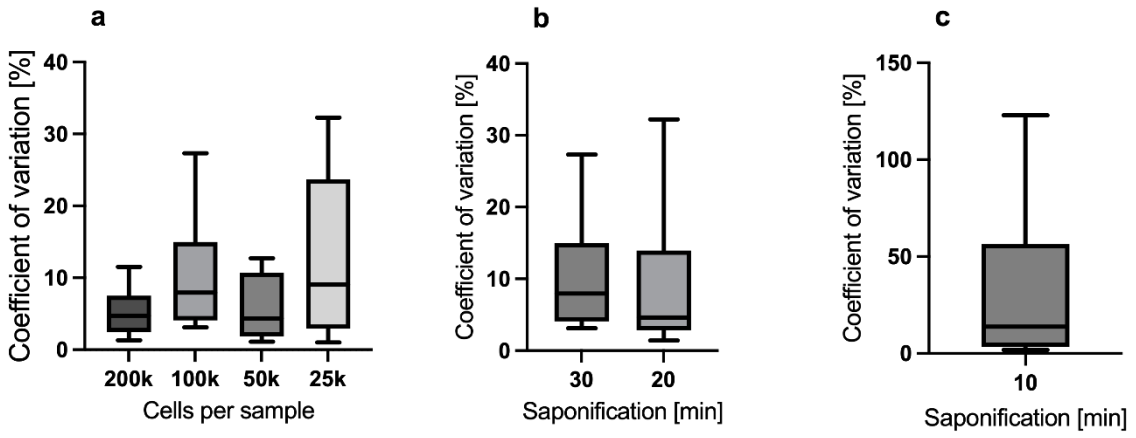

Figure 12: CVs of standards and median CV of different oxylipin extraction conditions. In a) varied cell densities per sample with a 30-minute-long saponification are depicted. In b) and c) varied lengths of saponification with samples of 10^5 cells per sample are illustrated.

In detail, the median CVs ranged from 4.4% to 13.8%. The CVs of all deuterated standards are summarized in Table 11. Taking the CVs of the standards into consideration, the overall optimal condition was identified to be the combination of a 20 min saponification a sample cell density of 10^5 cells per well.

Table 11: Median CVs of deuterated standards in different oxylipin extraction conditions

30 min saponification				100.000 cells		
200k	100k	50k	25k	30min	20min	10min
4,7%	8,0%	4,4%	9,1%	8,0%	4,6%	14%

To investigate the analyte pool of untreated whole cell lysates after saponification, abundance rank plots were performed. The mean normalized log_2 transformed areas under the curve of the control samples of the initial experiment conditions ($2*10^5$ cells $sample^{-1}$, 30-minute saponification) were ranked according to their relative abundance and are illustrated in Figure 13.

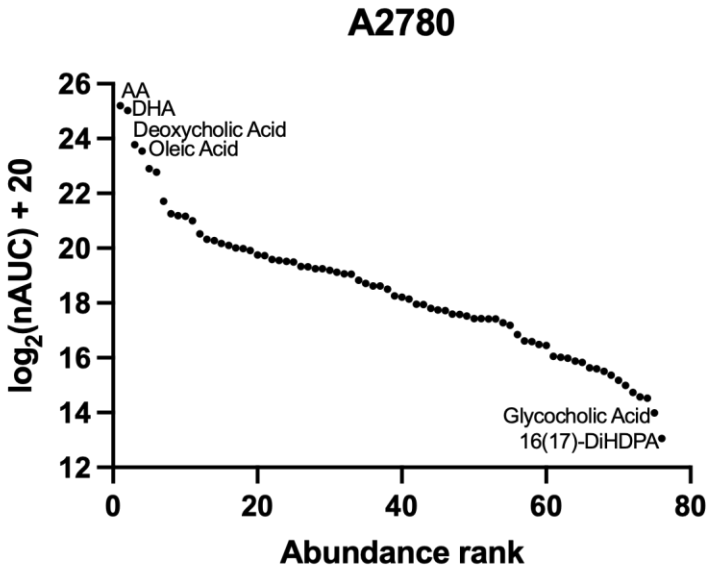

Figure 13: Abundance rank vs Log of all identified analytes in whole cell extracts after saponification.

The most abundant 4 analytes of whole A2780 cell lysates are AA, DHA, Deoxycholic acid and Oleic acid. AA and DHA are PUFAs and were expected to be among the most abundant species in cell membranes. As a reference, in human platelets, AA makes up about 25% of the phospholipid fatty acid content[107]. The bile acid Deoxycholic acid is a known promotor of colon cancer growth and progression[108]. Its high abundance in the ovarian cancer cell line A2780 may be an indicator, that it has a similar role in this type of cancer.

The different method conditions yielded trends of analyte levels depending on the method variables in both cell density and saponification length. PUFA levels tend to decrease with cell density. In Figure 14, this trend is illustrated with the examples of AA, DHA, DPA and EPA. Given their high abundance in cell membranes, PUFAs potentially might serve as parameters for cell density normalization.

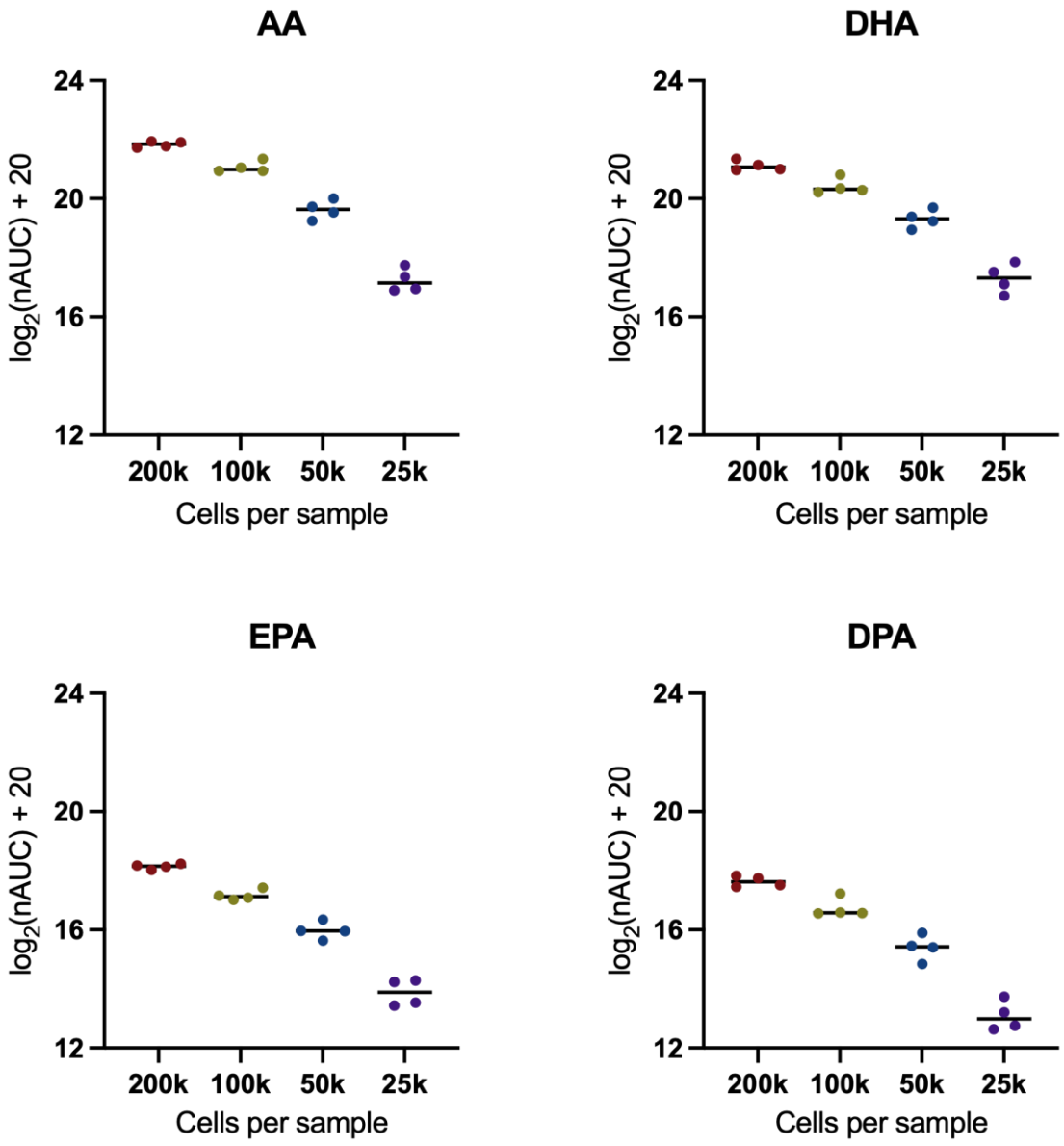

Figure 14: Log_2-transformed, normalized AUC of PUFAs versus cell density. Depicted are arachidonic acid (AA), Docosahexaenoic acid (DHA), Docosapentaenoic acid (DPA) and Eicosapentaenoic acid (EPA).

Another notable finding was the difference in oxylipin levels measured from extracts with different saponification periods. It can be noted, that some oxylipins decrease by increasing the saponification time. Exemplary oxylipins, in which this phenomenon was detected are illustrated in Figure 15.

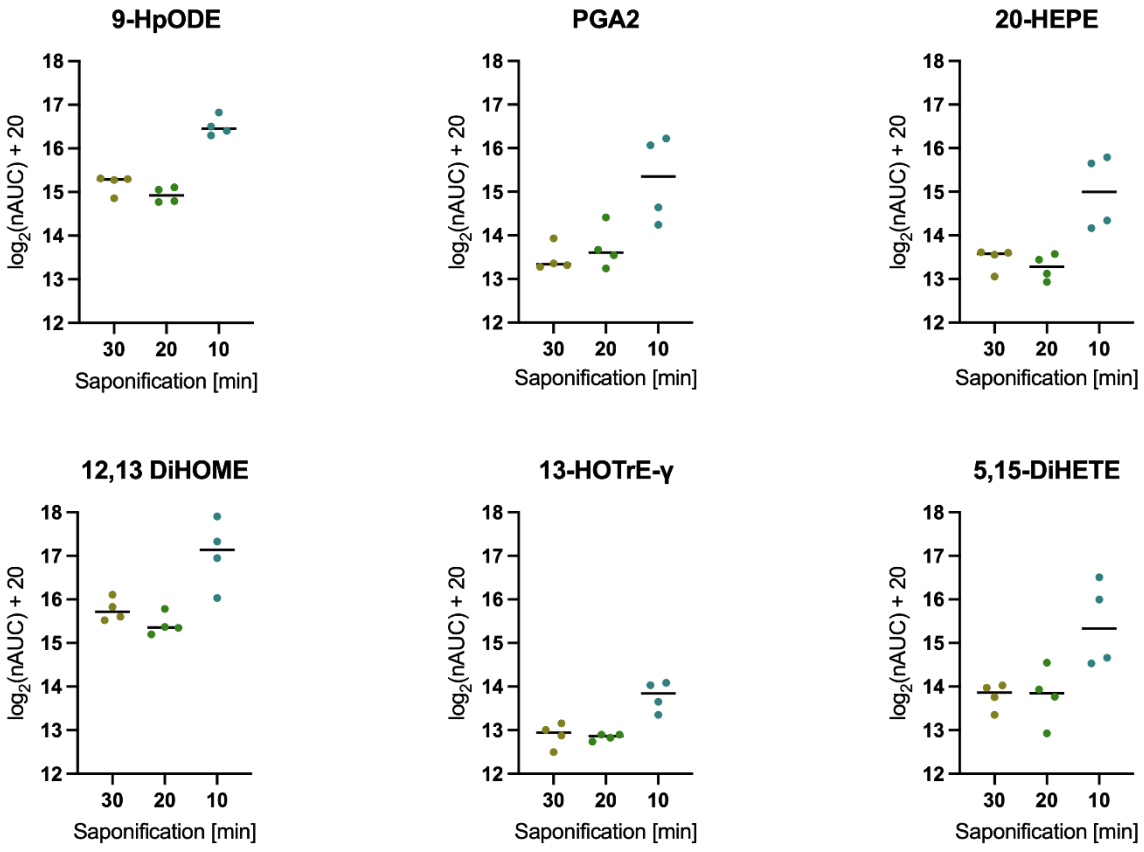

Figure 15: Log_2-transformed, normalized AUC of oxylipin precursors versus saponification length. Depicted are 9-HpODE; PGA2; 20-HEPE; 12,13 DiHOME; 13-HOTrE(gamma) and 5,15-DiHETE.

The increased levels of these analytes at shorter saponification periods are an indicator, that these undergo degradation during the process. A well-known example of such a degradation is the dehydration of prostaglandins in acidic and basic conditions[87]. However, throughout all extractions, several prostaglandin were detected.

4.3 Oxylipin profiles of regulated cell death in A2780 cells

In 2 iterations, the oxylipin profiles of A2780 undergoing RCD were investigated. Initially, A2780 cells were seeded at $2*10^5$ cells sample^{-1}, treated with cisplatin (9 µM) or RSL3 (106 nM) respectively and worked-up with a 30 min saponification. After investigation of different cell densities and saponification periods for the sample preparation, the cell density was adjusted to 10^5 cells and the saponification reduced to 20 min. Additionally, the treatment of RSL3 was reduced to 38 nM due to an increased sensitivity to RSL3, that was observed in the cell culture used for the second iteration of the experiment. Furthermore, a co-treatment of RSL3 (38 nM) and NDGA (4 µM) was investigated in the second iteration of the experiment. During the initial experiment, 75 analytes were identified. During second iteration with adjusted experimental conditions, 63 analytes were identified. They are all summarized in Table A 2. Significant down- and upregulations of oxylipins and their precursors were identified with a threshold of a Log_2(fold-change) > ±1 and a -Log_{10}(*p*-value) > 1.3.

4.3.1 Initial extraction and treatment conditions

In the initial iteration of the experiment, cells were treated with Cisplatin and RSL3 with $2*10^5$ cells per sample and a 30 min saponification. In Figure 16, the significant differences after RSL3 treatment in A2780 cells are visualized in the form of volcano plots.

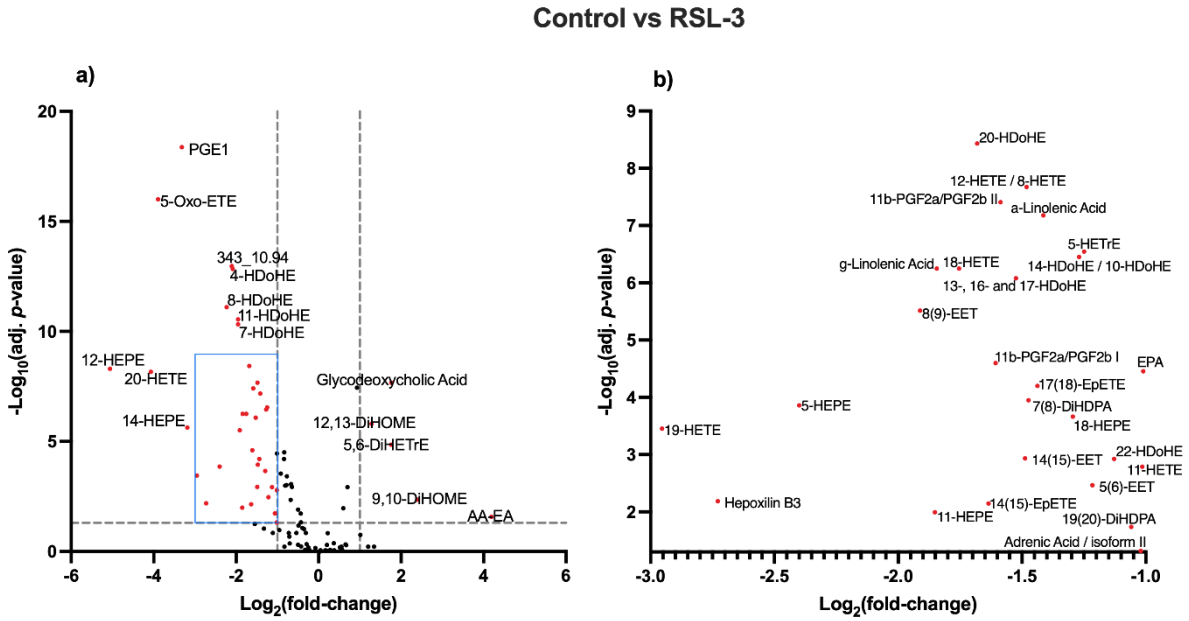

Figure 16: Volcano plots of A2780 cells in comparison with A2780 cells after 108 nM RSL3 treatment. Analytes with significant difference to the control are depicted as red dots, analytes with insignificant differences as black dots. In a), a volcano plot of all identified analytes is depicted. The range of log(fold-change) -1 to -3 and -log(P-value) < 9 is marked with a blue square. In b), analytes of this range are labelled and depicted in detail.

After RSL3 treatment, the levels of 9,10-DiHOME and 12,13-DiHOME increased significantly. They are the product of 9,10-EpOME and 12,13-EpOME hydrolysis mediated by soluble epoxide hydrolase (sEH)[109]. In a study, that investigated intracerebral hemorrhage of mice, inhibition of sEH reduced the rate of ferroptosis[110]. Furthermore, a decrease of all HDoHEs were detected upon RSL3 treatment. The levels of the majority of oxylipins and fatty acids decreased upon RSL3 treatment. Potentially, some of these are released into the cytoplasm to act as mediators in their free form during ferroptosis. An example for such a function is 20-HETE that acts as a pro-ferroptotic agent by decreasing the expression of GPX-4[79].

In Figure 17, the significant differences after Cisplatin treatment in A2780 cells are visualized in the form of volcano plots.

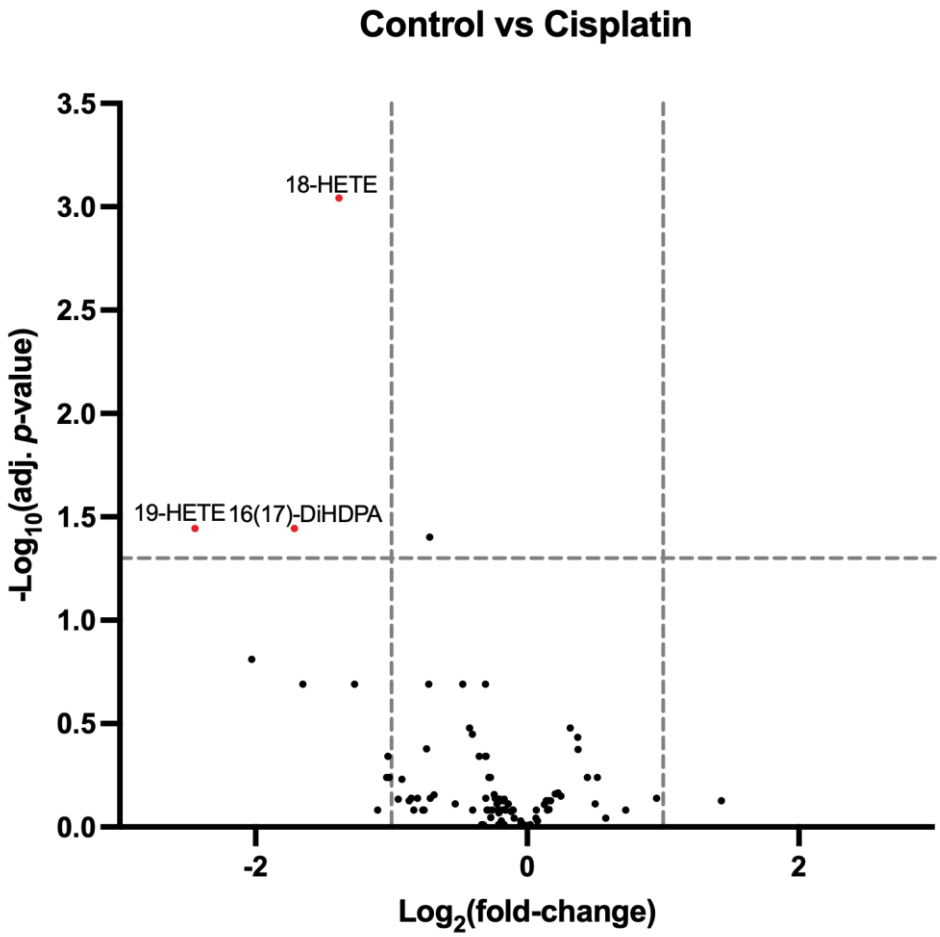

Figure 17: Volcano plot of A2780 cells in comparison with A2780 cells after 9µM cisplatin treatment. A volcano plot of all identified analytes is depicted. Analytes with significant difference to the control are depicted as red dots, analytes with insignificant differences as black dots.

Compared to the treatment with RSL3, it can be immediately noted, that less change in oxylipin profiles occurred upon Cisplatin treatment. What can be however noted, is that all 3 significantly downregulated species are products of CYP[1]. Interestingly, CYP ω-hydroxylases, that catalyze the formation of 18- and 19-HETE are known to have pro-apoptotic functions [111]. Therefore, it would be interesting to analyse free oxylipin levels to investigate, whether an increased signaling of these species takes place during apoptosis.

4.3.2 Adjusted extraction and treatment conditions

After investigation of the influence of cell density and duration of the saponification step on the method, the experiment was repeated with adapted conditions. The A2780 cell density was reduced to 10^5 cells per sample and the length of saponification from 30 min to 20 min. Furthermore, the RSL3 concentration was adapted to 38 nM and a co-treatment of RSL3 (38 nM) and NDGA (4µM) was additionally implemented. Due to technical problems, the RP-UHPLC separation method had to be changed, a new column (Phenomenex™ Kinetex™ XB-C18 column (150 x 2.1 mm, 1.7 µm,)) was used and the column oven temperature was changed from 40°C to 15°C. Significant down- and upregulations of oxylipins and their precursors were again identified with a threshold of a Log_2(fold-change) > ±1 and a -Log_{10}(*p*-value) > 1.3. In total, 63 analytes were identified during the second iteration of the experiment. The investigation of fatty acids and oxylipin profiles in ferroptosis and apoptosis led to inconsistent results in both treatments. Oxylipin levels of A2780 during RSL3 induced ferroptosis changed drastically from the first iteration of the experiment with a total of 41 significantly up- and down regulated analytes to the second iteration with only 4 significantly up-and down regulated analytes.

In Figure 18, the results of the cisplatin treatment are depicted. It can be noted, that in this experiment, nearly all analyte levels decreased.

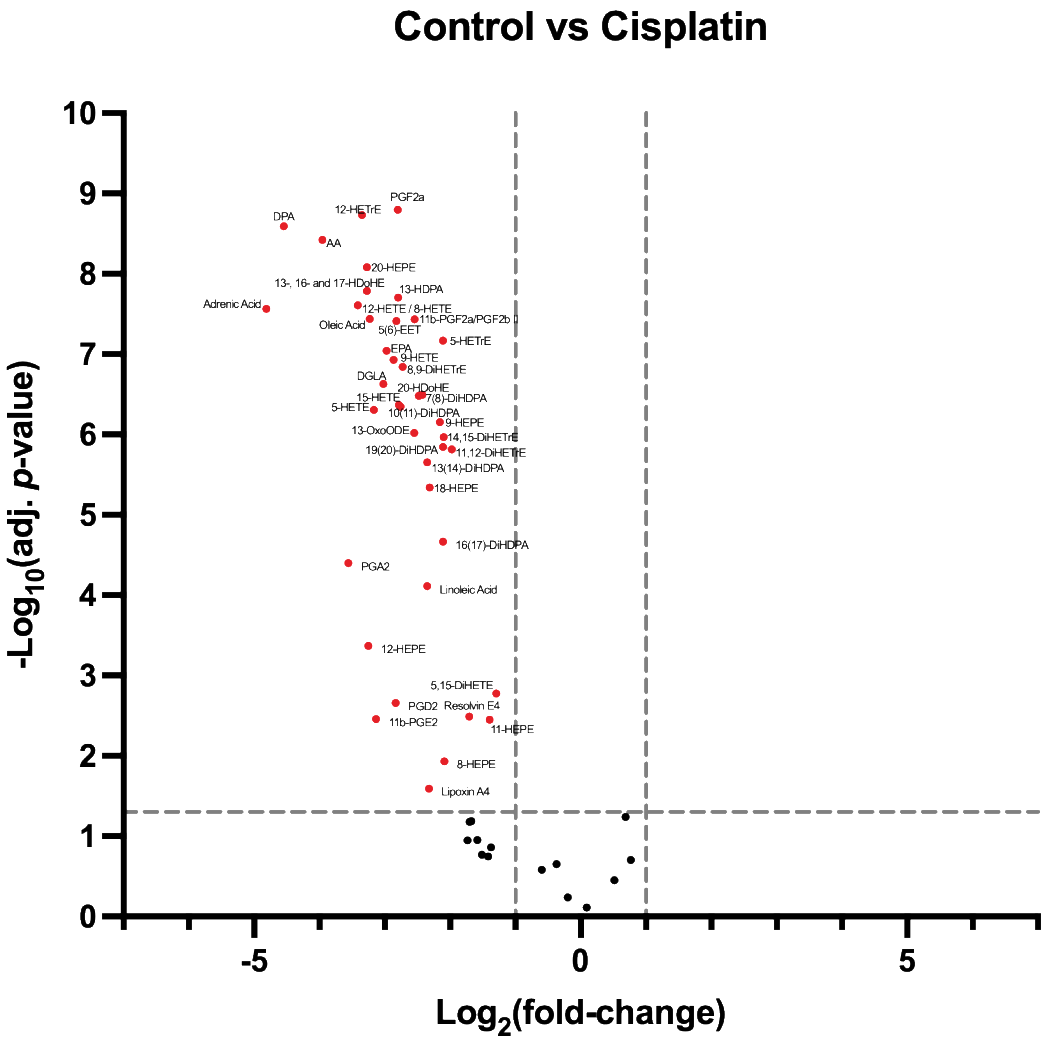

Figure 18: Volcano plot, A2780 cells after Cisplatin (9 µM). treatment compared to an untreated control lysate. Analytes with significant difference to the control are depicted as red dots, analytes with insignificant differences as black dots.

The highly significant, simultaneous and consistent decrease of the PUFAs AA, DPA AdA and linoleic acid combined with the decrease of nearly every singly analyte strongly suggests, that the overall cell density was lower than in the control cells. This was most likely caused by an elevated cytotoxicity.

In Figure 19, the significant up- and down regulations of fatty acids and oxylipins in the membrane fraction of A2780 cells after RSL3 (38 nM) treatment are illustrated.

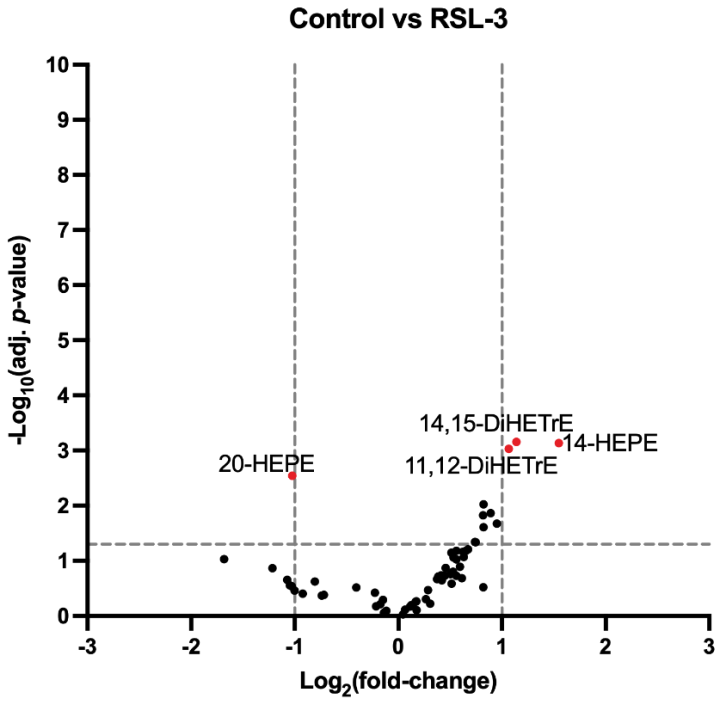

Figure 19 Volcano plot, A2780 cells after RSL3 (38 nM). treatment compared to an untreated control lysate. Analytes with significant difference to the control are depicted as red dots, analytes with insignificant differences as black dots.

In comparison to the initial experiment, the amount of significantly up- and downregulated oxylipins and fatty acids decreased. This was partially caused by a change of the UHPLC column leading to retention time shifts that made the detection of some analyte classes impossible due to the lack of a fitting compound database. Most prominently, out of the 6 HDoHEs (4-,7-,8-,11,20- and 22-HDoHE), only 20-HDoHE were identified. With the exception of the beforementioned HDoHEs, 5,6 DiHETrE and 5-Oxo-ETE however, all of the most significantly changed analytes of the initial iteration (analytes outside the range of log(fold-change) -1 to -3 and a -log(P-value) < 9 (summarized in Figure 16)a) were identified during the second iteration of the experiment. Yet, the same up and down regulation were not observed in the second iteration of the experiment. Potentially, the change in oxylipin regulation between the initial and second experiment were caused by the decrease of RSL3 concentration

from 108 nM to 38 nM. However, it can be noted, that 14,15-DiHETrE, 11,12-DiHETrE and 14-HEPE were upregulated upon RSL3 treatment while the level of 20-HEPE decreased. These up- and downregulations were not detected during the initial run of the experiment where 20-HEPE and 12,13-DiHETrE were not detected at all, 14,15-DiHETre had no significant change and 14-HEPE was downregulated. Interestingly, all of these compounds were CYP products. The donation of electrons to CYP by Cytochrome P450 reductase is potentially a crucial step for ferroptosis since Cytochrome P450 reductase elimination desensitizes cells drastically against ferroptosis. This further suggest the potential importance for CYP in ferroptosis[112]. To confirm a link between these CYP products and RSL3 induced ferroptosis, this experiment would have to be repeated.

To characterize the impact of 5-LOX inhibition on ferroptosis, the co-treatment of RSL3 and NDGA was investigated. Again, changes in oxylipin and fatty acid levels are visualized with volcano plots in Figure 20. Both, a comparison to the untreated control and the cells treated with only RSL3 were made.

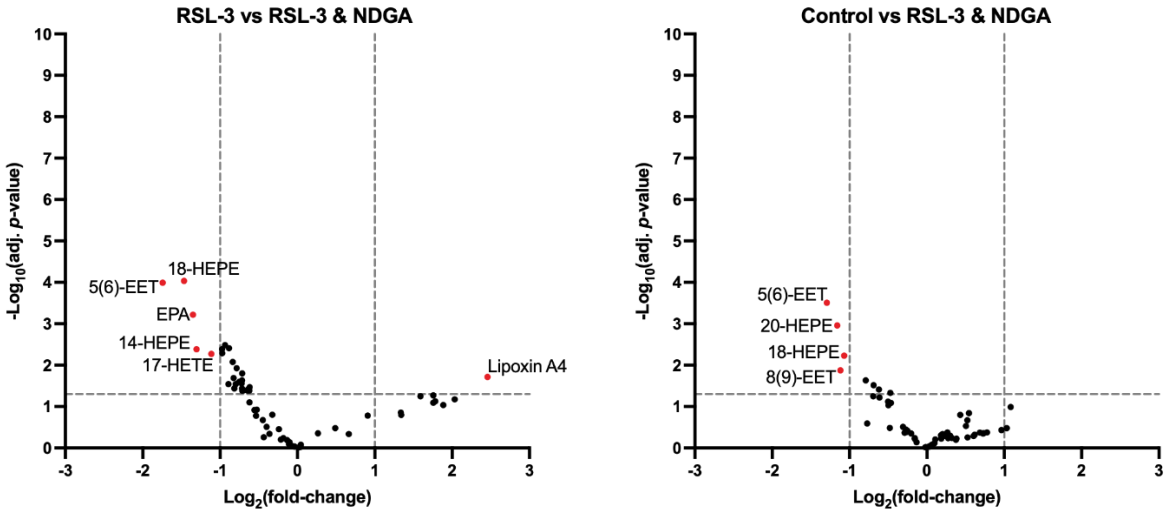

Figure 20: Volcano plots of A2780 cells after NDGA (4µM) co-treatment compared to just RSL3 (38 nM) and untreated controls. Analytes with significant difference to the control are depicted as red dots, analytes with insignificant differences as black dots.

Significant changes of oxylipin levels were detected in both, the comparison with the untreated control and the RSL3 treatment without NDGA. The levels of 5(6)-EET and 18-HEPE after RSL3 NDGA co-treatment are significantly lower in comparison to both, untreated control cells and RSL3 treatment without NDGA. The oxylipin 18-HEPE is known to suppress the chemokine receptor CXCR4 which is associated with melanoma progression. It thereby acts as a suppressor of melanoma metastasis[113]. EETs in general, are mediators for several physiological process like proliferation, migration, inflammation and tumor-angiogenesis. Further, the inhibition of CYP has shown to inhibit tumor angiogenesis[114].Further after RSL3 and NDGA co-treatment, the levels of 8(9)-EET and 20-HEPE decreased significantly in comparison to the untreated control cells and the levels of EPA, 14-HEPE and 17 HETE decreased significantly in comparison to the treatment with only RSL3. Lastly, upon RSL3 and NDGA co-treatment, Lipoxin A4 levels are significantly higher than in cells treated solely with RSL3. The exact opposite would have been expected since Lipoxin A4 is a downstream product of 5-LOX[1]. Curiously, with the exception of Lipoxin A4, the oxylipins that were identified and detected are CYP products[1].

[1]

4.4 Oxylipin profiles of A2780 mitochondria undergoing RCD

In the course of this project, it was investigated, whether mitochondrial membranes are a viable matrix for a saponification-based extraction of membrane bound oxylipins. A2780 cells were again used as model to investigate the role of oxylipins in mitochondrial membranes during apoptosis and ferroptosis. Analogously to the whole cell lysates, cells were treated with Cisplatin (9 µM) and RSL3 (38 nM). Per sample, $5*10^6$ cells were seeded, incubated for 24h and treated for another 24h. Before oxylipins were extracted (20 min saponification), mitochondria were extracted from the samples. In each treatment group the same 77 oxylipins and phospholipid precursors were identified.

Analogously to the whole cell lysates, the quality of the sample preparation and extraction was evaluated by the assessment of analyte and standard CVs. CVs of the

normalized analytes and of the 9 deuterated standards (Table 6 and Table 7) are visualized in Figure 21.

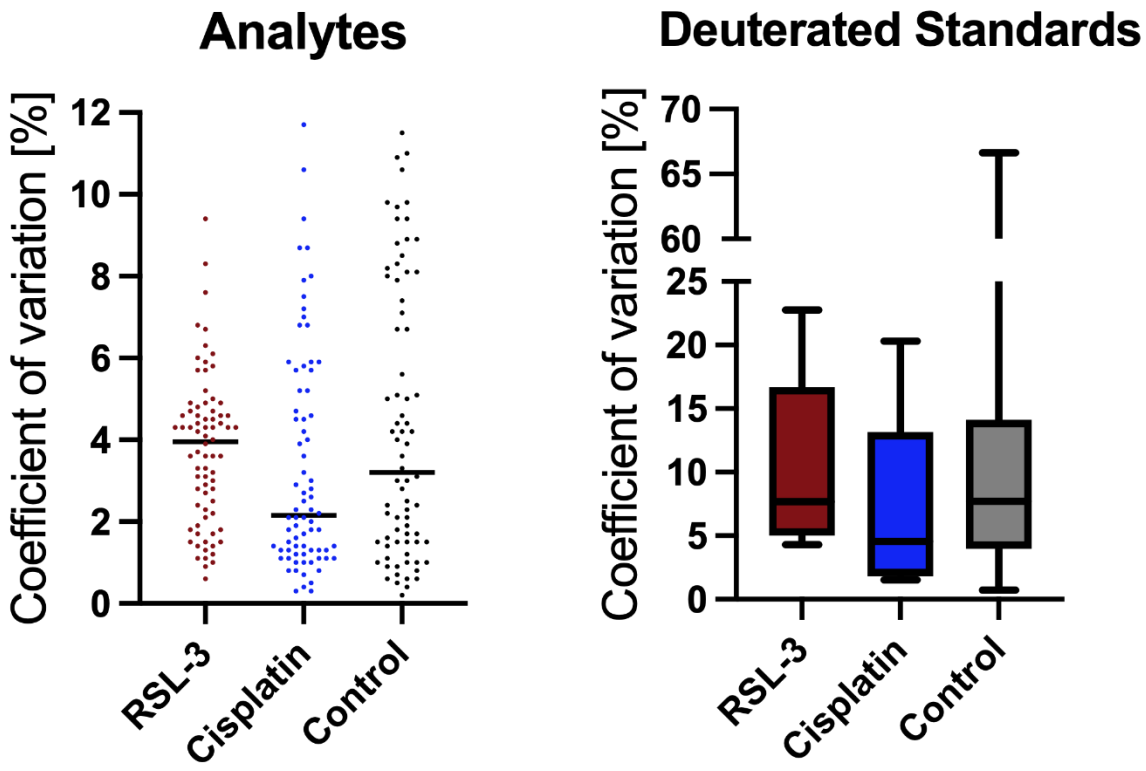

Figure 21: CVs of 77 identified, normalized analytes from A2780 mitochondrial fractions of RSL3 and Cisplatin treated cells with an additional untreated control group (left). CVs of all 9 deuterated standards (right).

From Figure 21, it can be deduced that the median CVs of the 77 identified analytes range between 2% and 4% in each treatment group CVs of individual analytes were all below 12%. With the exception of 5-Oxo-ETE-d7 in the control samples of 66,7 %, the CVs of all standards were below 25%. The median CVs in both, control samples and RSL3 treatments were 7,7% and the median CV of Cisplatin treated cells was 4,5%.

4.4.1 A2780 Mitochondria versus whole cell lysates

To investigate the analyte pool of mitochondria lysates after saponification, abundance rank plots of all control samples were performed. Here, the mean normalized, log_2 transformed areas under the curve of all control samples were ranked and illustrated in Figure 22.

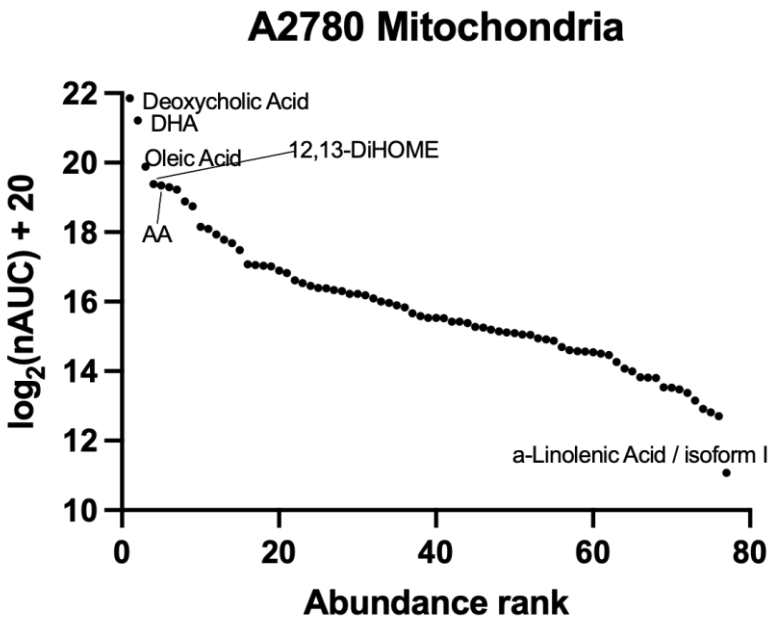

Figure 22: Abundance rank vs Log of all identified analytes in mitochondrial extracts after saponification.

In comparison to the whole cell lysates, it can be immediately noted, that the relative abundance of AA is lower in mitochondria. Furthermore, 12,13 DiHOME was the 4th most abundant analyte. 12,13 DiHOME is a mediator of several essential mitochondrial processes, for example it induces the expression of Nrf1(transcriptional regulator for mitochondrial biogenesis)[115,116].

To compare correlate the mitochondria and whole cell lysates the normalized, log_2 transformed areas under the curve of all control samples were directly correlated in a scatter plot illustrated in Figure 23.

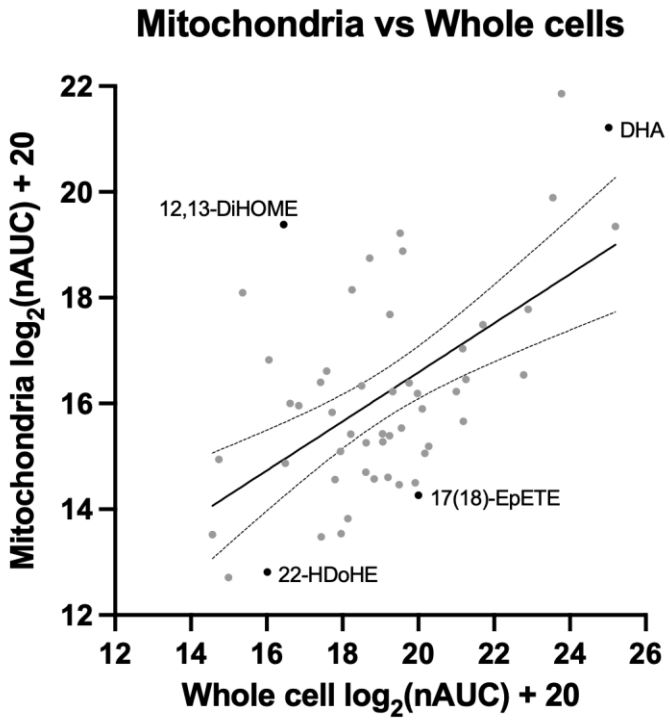

Figure 23: Scatter plot of all analytes that were present in the whole cell lysate and mitochondrial lysate of A2780 control cells after saponification. A linear regression with a confidence interval of 95% is indicated.

The analyte, that showed the highest relative difference between whole cells and mitochondrial fractions was 12,13-DiHOME which aligns with the findings of the abundance ranks. An analyte that was significantly higher than the regression trend in the whole cell lysates was 17(18)-EpETE. Functionally, 17(18)-EpETE is an activator of big potassium calcium channels (BK_{Ca}) thereby regulating membrane potentials[117]. Multiple isoforms of BK_{Ca} exist, that are located both in cell membranes and the mitochondrial membranes and differ in sensitivity to voltage[118]. Finally, an interesting trend between 22-HDoHE and its precursor DHA can be deducted. While DHA is elevated in mitochondria, 22-HDoHE levels are lower in comparison to the whole cell-lysates.

4.4.2 Oxylipin and fatty acid profiles of mitochondrial membranes during RCD

Analogously to the investigation of RCDs in, whole cell lysates the significant differences in analyte levels after cisplatin and RSL3 treatment were analyzed. The same thresholds of Log_2(fold-change) > ±1 and a -Log_{10}(*p*-value) > 1.3 were applied. The results are depicted in the volcano plots of Figure 24.

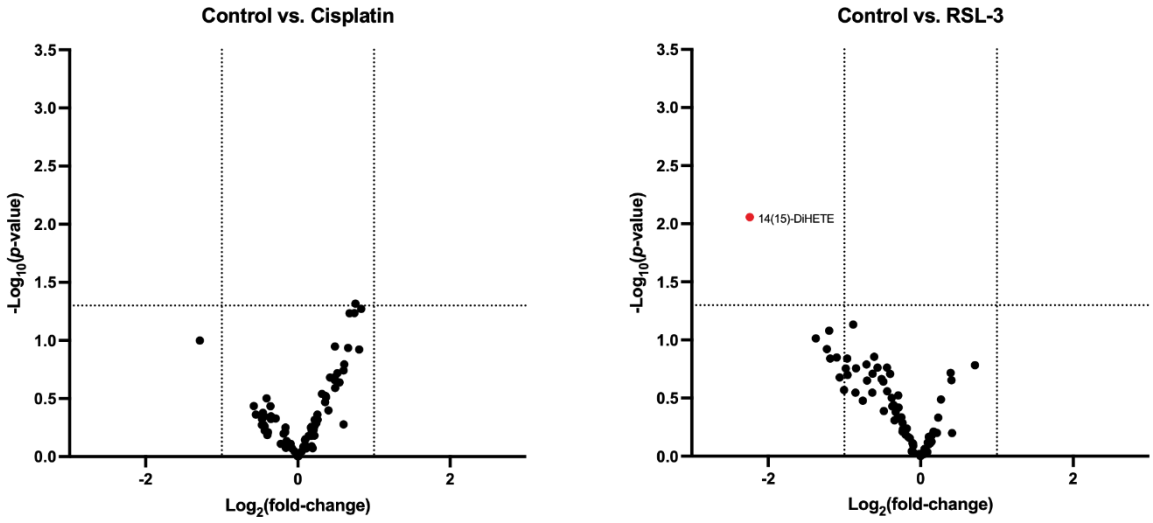

Figure 24: Volcano plots of A2780 mitochondria after Cisplatin (9 µM) and RSL3 (38 nM) treatment. Analytes with significant difference to the control are depicted as red dots, analytes with insignificant differences as black dots.

A significant decrease in 14(15)-DiHETE levels were detected in the mitochondrial fraction after RSL3 treatment. Interestingly, neither a mitochondria- nor a ferroptosis-specific relation with 14(15)-DiHETE has been drawn yet in other research. However interestingly, 14(15)-DiHETE is a CYP product[1] which further draws attention to the findings of the second iteration of the A2780 whole cell lysates after RSL3 treatment, depicted in Figure 19, where also only upregulations of CYP products were observed.

In Figure 25, the 14(15)-DiHETE levels of all replicates are depicted. While 14(15)-DiHETE levels were significantly reduced in ferroptosis, it must be stated, that the variance of 14(15)-DiHETE levels was high in the control cells.

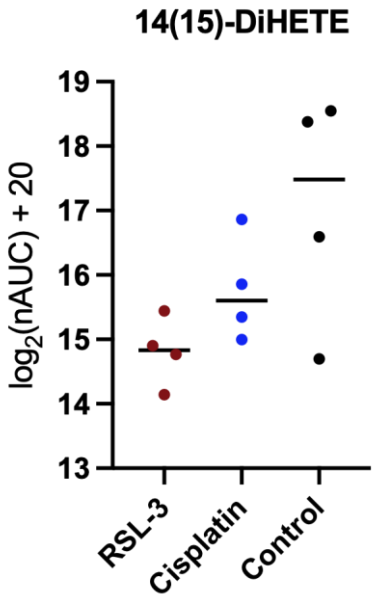

Figure 25: 14(15)-DiHETE levels in the mitochondrial fraction after RSL3 and Cisplatin treatment with medians.

4.5 Oxylipin and fatty acid profiles of HL-60 cells upon differentiation

The fatty acid and oxylipin profiles of HL-60 cells were investigated during differentiation induced with ATRA and DMSO respectively. During both treatments, cells were additionally stimulated with TGF-β1. Additionally, an ATRA treatment without TGF-β1 was performed. In total, 77 analytes were identified in the samples after ATRA treatment and 67 after DMSO treatment. The results are here again illustrated in the form of volcano plots in Figure 26.

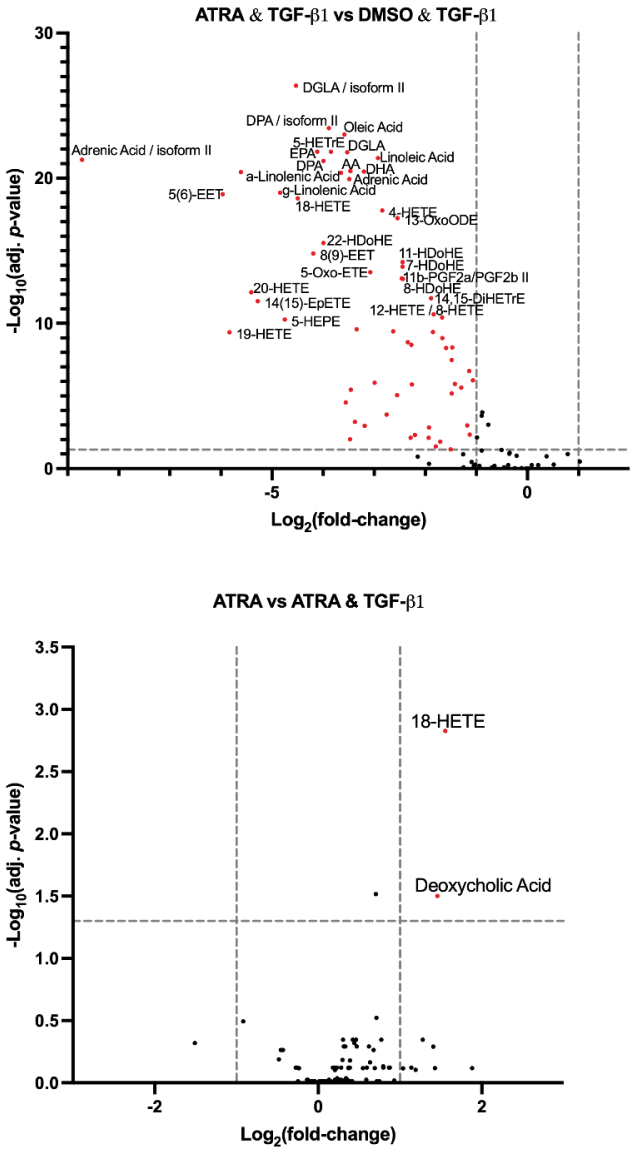

Figure 26: Volcano plots, fatty acids and oxylipins of HL-60 membranes upon ATRA and DMSO treatment with TGF-β1 stimulation (left). ATRA treatment with and without TGF-β1 stimulation (right)

The differentiation of HL-60 cells caused partial adherence, which complicated the extraction process and did not allow proper comparison with untreated control cells. It however can be observed, that nearly all analyte levels are significantly lower in HL-60 cells treated with DMSO in comparison to HL-60 treated with ATRA. By molecular dynamics simulations, it was explored, that DMSO has causes the thinning of lipid membranes[119] which might explain this strong decrease and the complete lack of any significant upregulation. Furthermore, in comparison to a pure ATRA treatment, it can be deducted that an ATRA and TGF-β1 cotreatment lead to increased levels of 18-HETE and Deoxycholic acid.

5. Conclusion and outlook

The main objective of this thesis was to implement a method for saponification-based extraction of membrane-bound oxylipins and fatty acids from human cancer cell lines. This method was adapted to an in-house untargeted LC-MS workflow and used to characterize fatty acids and oxylipins. The validity of the approach was evaluated in whole cell lysates of two different biological model systems, the ovarian cancer cell line A2780 and the promyelocytic leukemia cell line HL-60. Further, the method was also evaluated in crude mitochondrial fractions of A2780 cells. The method successfully was used to characterize between ≥63 analytes in A2780 cells and ≥67 in HL-60 cells.

The saponification method was optimized with respect to saponification time and cell numbers per well to decrease the variance of the analytes and standards. During the preliminary method, a 30 min long saponification period was performed on samples seeded with $2*10^5$ cells per well, which yielded a median analyte CV of 2,6%. The optimal condition was identified as a 20 min long saponification with a cell density of 10^5 cells per well that yielded a median analyte CV of 2,3%. Summarizing, the method improved method were time expenditure and required cell amount and analyte variation were all decreased. During the investigation of the methodic parameters, it became apparent, that the abundancies of several compounds decrease with increasing saponification periods. This trend was observed throughout several classes of oxylipins and PUFAS such as in 9-HpODE, PGA2, 20-HEPE, 12,13 DiHOME, 13-HOTrE- γ and 5,15-DiHETE indicating a certain degree of degradation of analytes during saponification that should be evaluated in subsequent studies. Additionally, it was observed, that cell density for membrane bound oxylipin analysis has an apparent correlation between levels of the PUFAs such as AA, DHA and DPA and number of cells per well. This potentially might lead the way to a cell density normalization approach for future projects that focus on the characterization of fatty acids or oxylipins in cell culture.

The method was then further utilized to characterize two different biological systems, the hematopoietic differentiation of HL-60 cells induced by DMSO and ATRA respectively and regulated cell death in the form of apoptosis and ferroptosis in A2780 cells. The investigation of the HL-60 cells most notably provided more indications towards a membrane thinning effect of DMSO which has been proposed by molecular dynamics simulations. It would be promising to further investigate the DMSO induced cell thinning with our extraction method on different cell lines.

The intent behind analyzing membrane bound oxylipin levels of cells undergoing regulated cell death was to uncover distinct regulatory oxylipins of ferroptosis which is hypothesized to be a process mainly driven by lipid peroxidation. Upon RSL-3 induced ferroptosis, four significantly up and downregulated analytes were identified with the optimized saponification method. During ferroptosis, 14-HEPE 14,15-DiHETE and 11,12-DiHETrE were upregulated while 20 HEPE was downregulated. After a co-treatment of RSL3 with the LOX inhibitor NDGA, 5(6)-EET and 18-HEPE levels decreased in comparison to both control cells and RSL3-only treated cells. Upon Cisplatin-induced apoptosis, 18-HETE, 19-HETE and 16(17)-DiHDPA were identified downregulations in the first iteration of the experiment. In the second one, Cisplatin-induced apoptosis leaded to a significant decrease of almost every analyte level including several PUFAs which indicates a decreased cell density in the samples.

Interestingly, during both regulated cell death processes, a majority of analytes, that underwent regulatory changes were CYP products. This potential prevalence of a CYP dependent regulation during regulated cell death must be confirmed by additional repetitions of this experiment.

In summary, the saponification-based extraction method presented here is an effective method to extract fatty acids and oxylipins from membranes. It can be implemented to perform untargeted analysis of oxylipin and fatty acid profiles and proves useful for a variety of biological systems. The method has proven as fairly robust and can give insights into both complex lipid mediation systems and structural changes involving membranes.

6. References

1. Melissa Gabbs, Leng, S., Devassy, J. G., Monirujjaman, M. & Aukema, H. M. Advances in our understanding of oxylipins derived from Dietary PUFAs. *Adv Nutr* **6**, 513–540 (2015).
2. Yamaguchi, A., Botta, E. & Holinstat, M. Eicosanoids in inflammation in the blood and the vessel. *Front Pharmacol* **13**, 997403 (2022).
3. Sisemore, M. F. *et al.* Cellular characterization of leukotoxin diol-induced mitochondrial dysfunction. *Arch Biochem Biophys* **392**, 32–37 (2001).
4. Wang, D. & Dubois, R. N. Eicosanoids and cancer. *Nat Rev Cancer* **10**, 181–193 (2010).
5. Markworth, J. F., Krishna, R. M. & Cameron-Smith, D. Emerging roles of pro-resolving lipid mediators in immunological and adaptive responses to exercise-induced muscle injury. *Exerc Immunol Rev* **22**, 110–134 (2016).
6. Schebb, N. H. *et al.* Comparison of the effects of long-chain omega-3 fatty acid supplementation on plasma levels of free and esterified oxylipins. *Prostaglandins Other Lipid Mediat* **113–115**, 21–29 (2014).
7. Kock, J. L. F., Sebolai, O. M., Pohl, C. H., Van Wyk, P. W. J. & Lodolo, E. J. Oxylipin studies expose aspirin as antifungal. *FEMS Yeast Res* **7**, 1207–1217 (2007).
8. Roy Baker, R. The eicosanoids: A historical overview. *Clin Biochem* **23**, 455–458 (1990).
9. The Nobel Prize in Physiology or Medicine 1982. https://www.nobelprize.org/prizes/medicine/1982/summary/.
10. Bergström, S., Ryhage, R., Samuelsson, B. & Sjövall, J. Prostaglandins and related factors. *J Biochem* **238**, 3555–3564 (1963).
11. Bergström, S., Danielsson, H. & Samuelsson, B. The enzymatic formation of prostaglandin E2 from arachidonic acid prostaglandins and related factors 32. *Biochim Biophys Acta* **90**, 207–210 (1964).
12. Vane, J. R. Inhibition of Prostaglandin Synthesis as a Mechanism of Action for Aspirin-like Drugs. *Nat New Biol* **231**, 232–235 (1971).
13. Goodarzi, K., Goodarzi, M., Tager, A. M., Luster, A. D. & von Andrian, U. H. Leukotriene B4 and BLT1 control cytotoxic effector T cell recruitment to inflamed tissues. *Nat Immunol* **4**, 965–973 (2003).
14. Hijioka, M. *et al.* Microglia-released leukotriene B4 promotes neutrophil infiltration and microglial activation following intracerebral hemorrhage. *Int Immunopharmacol* **85**, 106678 (2020).
15. O'Donnell, V. B., Aldrovandi, M., Murphy, R. C. & Krönke, G. Enzymatically oxidized phospholipids assume center stage as essential regulators of innate immunity and cell death. *Sci Signal* **12**, 2293 (2019).
16. Goodsell, D. S. The Molecular Perspective: Cytochrome c and Apoptosis; The Molecular Perspective: Cytochrome c and Apoptosis. *Oncologist* **9**, 226–227 (2004).
17. Conroy, M. J. *et al.* LIPID MAPS: update to databases and tools for the lipidomics community. *Nucleic Acids Res* **52**, D1677–D1682 (2024).
18. Akefe Isaac O. Wallis Tristan P., Osborne, S. L., Matthews Benjamin, Wallis Tristan P. & Meunier Frédéric A. Lipids and secretory vesicle exocytosis. *Adv Neurobiol* **33**, 357–397 (2023).

19. Ghosh, M., Tucker, D. E., Burchett, S. A. & Leslie, C. C. Properties of the group IV phospholipase A2 family. *Prog Lipid Res* **45**, 487–510 (2006).
20. Petan, T. & Manček-Keber, M. Half is enough: Oxidized lysophospholipids as novel bioactive molecules. *Free Radic Biol Med* **188**, 351–362 (2022).
21. Hellhake, S. *et al.* Non-targeted and targeted analysis of oxylipins in combination with charge-switch derivatization by ion mobility high-resolution mass spectrometry. *Anal Bioanal Chem* **412**, 5743–5757 (2020).
22. Liu, Y. & Roth, J. P. A revised mechanism for human cyclooxygenase-2. *J Biol Chem* **291**, 948–958 (2016).
23. Hla, T., Bishop-Bailey, D., Liu, C. H., Schaefers, H. J. & Trifan, O. C. Cyclooxygenase-1 and -2 isoenzymes. *Int J Biochem Cell Biol* **31**, 551–557 (1999).
24. Brooks, P. *et al.* Interpreting the clinical significance of the differential inhibition of cyclooxygenase-1 and cyclooxygenase-2. *Rheumatology* **38**, 779–788 (1999).
25. Vane, J. R. & Botting, R. M. New insights into the mode of action of anti-inflammatory drugs. *Inflamm Res* **44**, 1–10 (1995).
26. Gilroy, D. W. & Colville-Nash, P. R. New insights into the role of COX 2 in inflammation. *J Mol Med* **78**, 121–129 (2000).
27. Rowlinson, S. W., Crews, B. C., Lanzo, C. A. & Marnett, L. J. The binding of arachidonic acid in the cyclooxygenase active site of mouse prostaglandin endoperoxide synthase-2 (COX-2). A putative L-shaped binding conformation utilizing the top channel region. *J Biol Chem* **274**, 23305–23310 (1999).
28. Smith, W. L., DeWitt, D. L. & Garavito, R. M. Cyclooxygenases: Structural, cellular, and molecular biology. *Annu Rev Biochem* **69**, 145–182 (2000).
29. Ricciotti, E. & Fitzgerald, G. A. Prostaglandins and Inflammation. *Arterioscler Thromb Vasc Biol* **31**, 986–1000 (2011).
30. Vliegenthart, J. F. G. & Veldink, G. A. Substrates and products of lipoxygenase catalysis. *Stud Nat Prod Chem* **9**, 559–589 (1991).
31. Yamamoto, S. Mammalian lipoxygenases: molecular structures and functions. *Biochim Biophys Acta* **1128**, 117–131 (1992).
32. Orafaie, A., Mousavian, M., Orafai, H. & Sadeghian, H. An overview of lipoxygenase inhibitors with approach of in vivo studies. *Prostag oth lipid m* **148**, 106411 (2020).
33. Powell, W. S. & Rokach, J. Biosynthesis, biological effects, and receptors of hydroxyeicosatetraenoic acids (HETEs) and oxoeicosatetraenoic acids (oxo-ETEs) derived from arachidonic acid. *Biochim Biophys Acta* **1851**, 340–355 (2015).
34. Gilbert, N. C., Newcomer, M. E. & Werz, O. Untangling the web of 5-lipoxygenase-derived products from a molecular and structural perspective: The battle between pro- and anti-inflammatory lipid mediators. *Biochem Pharmacol* **193**, 114759 (2021).
35. Nebert, D. W. & Russell, D. W. Clinical importance of the cytochromes P450. *Lancet* **360**, 1155–1162 (2002).
36. Hardwick, J. P. Cytochrome P450 omega hydroxylase (CYP4) function in fatty acid metabolism and metabolic diseases. *Biochem Pharmacol* **75**, 2263–2275 (2008).
37. Spector, A. A. & Kim, H. Y. Cytochrome P450 epoxygenase pathway of polyunsaturated fatty acid metabolism. *Biochim Biophys Acta* **1851**, 356 (2015).
38. Spector, A. A. Arachidonic acid cytochrome P450 epoxygenase pathway. *J Lipid Res* **50**, S52–S56 (2009).

39. Campbell, W. B. & Falck, J. R. Arachidonic acid metabolites as endothelium-derived hyperpolarizing factors. *Hypertens* **49**, 590–596 (2007).
40. Spiecker, M. & Liao, J. K. Vascular protective effects of cytochrome p450 epoxygenase-derived eicosanoids. *Arch Biochem Biophys* **433**, 413–420 (2005).
41. Moran, J. H., Weise, R., Schnellmann, R. G., Freeman, J. P. & Grant, D. F. Cytotoxicity of linoleic acid diols to renal proximal tubular cells. *Toxicol Appl Pharmacol* **146**, 53–59 (1997).
42. Yin, H., Xu, L. & Porter, N. A. Free radical lipid peroxidation: Mechanisms and analysis. *Chem Rev* **111**, 5944–5972 (2011).
43. Ingold, K. U. Peroxy Radicals. *Acc Chem Res* **2**, 1–9 (1969).
44. Gardner, H. W. Oxygen radical chemistry of polyunsaturated fatty acids. *Free Radic Biol Med* **7**, 65–86 (1989).
45. Do, Q. *et al.* Development and application of a peroxyl radical clock approach for measuring both hydrogen-atom transfer and peroxyl radical addition rate constants. *Journal of Organic Chemistry* **86**, 153–168 (2021).
46. Roberts, L. J. & Milne, G. L. Isoprostanes. *J Lipid Res* **50**, S219–S223 (2009).
47. Milne, G. L., Yin, H., Hardy, K. D., Davies, S. S. & Roberts, L. J. Isoprostane generation and function. *Chem Rev* **111**, 5973–5996 (2011).
48. Yi, C. *et al.* Activation of orphan receptor GPR132 induces cell differentiation in acute myeloid leukemia. *Cell Death Dis* **13**, 1–15 (2022).
49. Lahvic, J. L. *et al.* Specific oxylipins enhance vertebrate hematopoiesis via the receptor GPR132. *Proc Natl Acad Sci U S A* **115**, 9252–9257 (2018).
50. Kawamoto, H. & Minato, N. Myeloid cells. *Int J Biochem Cell Biol* **36**, 1374–1379 (2004).
51. De Kleer, I., Willems, F., Lambrecht, B. & Goriely, S. Ontogeny of myeloid cells. *Front Immunol* **5**, 110421 (2014).
52. Weiskopf, K. *et al.* Myeloid cell origins, differentiation, and clinical implications. *Microbiol Spectr* **4**, (2016).
53. Saluja, S., Bansal, I., Bhardwaj, R., Beg, M. S. & Palanichamy, J. K. Inflammation as a driver of hematological malignancies. *Front Oncol* **14**, 1347402 (2024).
54. Tasseff, R. *et al.* An effective model of the retinoic acid induced HL-60 differentiation program. *Sci Rep* **7**, 1–21 (2017).
55. Lo-Coco, F. *et al.* Retinoic acid and arsenic trioxide for acute promyelocytic leukemia. *N Engl J Med* **369**, 111–121 (2013).
56. Ennaciri, J. & Girard, D. Immune system: maturation of myeloid cells. *Methods Mol Biol* **550**, 195–203 (2009).
57. Manda-Handzlik, A. *et al.* The influence of agents differentiating HL-60 cells toward granulocyte-like cells on their ability to release neutrophil extracellular traps. *Immunol Cell Biol* **96**, 413–425 (2018).
58. Dong, X. *et al.* ATRA treatment slowed P-selectin-mediated rolling of flowing HL60 cells in a mechano-chemical-dependent manner. *Front Immunol* **14**, 1148543 (2023).
59. Lee, E., Song, C.-H., Bae, S.-J., Ha, K.-T. & Karki, R. Regulated cell death pathways and their roles in homeostasis, infection, inflammation, and tumorigenesis. *Exp Mol Med* **55**, 1632–1643 (2023).
60. Green, D. R. The coming decade of cell death research: Five riddles. *Cell* **177**, 1094–1107 (2019).

61. Jin, X. *et al.* Ferroptosis: Emerging mechanisms, biological function, and therapeutic potential in cancer and inflammation. *Cell Death Discov* **10**, (2024).
62. Sun, E. W. & Shi, Y. F. Apoptosis: the quiet death silences the immune system. *Pharmacol Ther* **92**, 135–145 (2001).
63. Nagata, S. Apoptosis and clearance of apoptotic cells. *Annu Rev Immunol* **36**, 489–517 (2018).
64. Kerr, J. F. R., Wyllie, A. H. & Currie, A. R. Apoptosis: a basic biological phenomenon with wide-ranging implications in tissue kinetics. *Br. J. Cancer* **26**, 239 (1972).
65. Brill, A., Torchinsky, A., Carp, H. & Toder, V. The role of apoptosis in normal and abnormal embryonic development. *J Assist Reprod Genet* **16**, 512–519 (1999).
66. Zia, Q. *et al.* Cell death: A molecular perspective. *Curr Mol Biol Rep* **7**, 41–66 (2021).
67. Nagata, S. Apoptosis and clearance of apoptotic cells. *Annu Rev Immunol* **36**, 489–517 (2018).
68. Basu, A. & Krishnamurthy, S. Cellular responses to cisplatin-induced DNA damage. *J Nucleic Acids* **2010**, (2010).
69. Green, D. R. The death receptor pathway of apoptosis. *Cold Spring Harb Perspect Biol* **14**, (2022).
70. Segawa, K. & Nagata, S. An apoptotic 'eat me' signal: phosphatidylserine exposure. *Trends Cell Biol* **25**, 639–650 (2015).
71. Dixon, S. J. *et al.* Ferroptosis: An iron-dependent form of nonapoptotic cell death. *Cell* **149**, 1060–1072 (2012).
72. Probst, L., Dächert, J., Schenk, B. & Fulda, S. Lipoxygenase inhibitors protect acute lymphoblastic leukemia cells from ferroptotic cell death. *Biochem Pharmacol* **140**, 41–52 (2017).
73. Agmon, E., Solon, J., Bassereau, P. & Stockwell, B. R. Modeling the effects of lipid peroxidation during ferroptosis on membrane properties. *Sci Rep* **8**, (2018).
74. Reddanna, P., Krishna Rao, M. & Channa Reddy, C. Inhibition of 5-lipoxygenase by vitamin E. *FEBS Lett* **193**, 39–43 (1985).
75. Zilka, O. *et al.* On the mechanism of cytoprotection by ferrostatin-1 and liproxstatin-1 and the role of lipid peroxidation in ferroptotic cell death. *ACS Cent Sci* **3**, 232–243 (2017).
76. Xie, Y., Kang, R., Klionsky, D. J. & Tang, D. GPX4 in cell death, autophagy, and disease. *Autophagy* **19**, 2621–2638 (2023).
77. Sato, M. *et al.* The ferroptosis inducer erastin irreversibly inhibits system xc− and synergizes with cisplatin to increase cisplatin's cytotoxicity in cancer cells. *Sci Rep* **8**, 1–9 (2018).
78. Yang, W. S. *et al.* Regulation of ferroptotic cancer cell death by GPX4. *Cell* **156**, 317–331 (2014).
79. Han, R. *et al.* 20-HETE participates in intracerebral hemorrhage-induced acute injury by promoting cell ferroptosis. *Front Neurol* **12**, 763419 (2021).
80. (1S,3R)-RSL3. https://www.biomol.com/de/produkte/chemikalien/biochemikalien/1s-3r-rsl3-cay19288-1#.
81. Nordihydroguaiaretic Acid. *retrieved: 12.6.2024* https://www.biomol.com/de/produkte/chemikalien/lipide/nordihydroguaiaretic-acid-cay70300-500.

82. Doll, S. *et al.* ACSL4 dictates ferroptosis sensitivity by shaping cellular lipid composition. *Nat Chem Biol* **13**, 91–98 (2016).
83. Hou, J. *et al.* ACSL4 as a potential target and biomarker for anticancer: From molecular mechanisms to clinical therapeutics. *Front Pharmacol* **13**, 949863 (2022).
84. Dixon, S. J. & Stockwell, B. R. The hallmarks of ferroptosis. *Annu Rev Cancer Biol* **3**, 35–54 (2019).
85. Li, B. *et al.* Emerging mechanisms and applications of ferroptosis in the treatment of resistant cancers. *Biomed Pharmacother* **130**, 110710 (2020).
86. Liakh, I., Pakiet, A., Sledzinski, T. & Mika, A. Modern methods of sample preparation for the analysis of oxylipins in biological samples. *Molecules* **24**, 1639 (2019).
87. Quehenberger, O., Dahlberg-Wright, S., Jiang, J., Armando, A. M. & Dennis, E. A. Quantitative determination of esterified eicosanoids and related oxygenated metabolites after base hydrolysis. *J Lipid Res* **59**, 2436–2445 (2018).
88. Wang, T. *et al.* A rapid and high-throughput approach to quantify non-esterified oxylipins for epidemiological studies using online SPE-LC-MS/MS. *Anal Bioanal Chem* **412**, 7989–8001 (2020).
89. Nayeem, M. A. Role of oxylipins in cardiovascular diseases. *Acta Pharmacol Sin* **39**, 1142–1154 (2018).
90. Eibl, H. Phospholipids as Functional Constituents of Biomembranes. *Angewandte Chemie International Edition in English* **23**, 257–271 (1984).
91. Prieto Vidal, N. *et al.* The effects of cold saponification on the unsaponified fatty acid composition and sensory perception of commercial natural herbal soaps. *Molecules* **23**, 2356 (2018).
92. Poole, C. F. New trends in solid-phase extraction. *TrAC Trends in Analytical Chemistry* **22**, 362–373 (2003).
93. Gladine, C., Ostermann, A. I., Newman, J. W. & Schebb, N. H. MS-based targeted metabolomics of eicosanoids and other oxylipins: Analytical and inter-individual variabilities. *Free Radic Biol Med* **144**, 72–89 (2019).
94. Dasilva, G. *et al.* Lipidomic analysis of polyunsaturated fatty acids and their oxygenated metabolites in plasma by solid-phase extraction followed by LC-MS. *Anal Bioanal Chem* **406**, 2827–2839 (2014).
95. Liakh, I., Pakiet, A., Sledzinski, T. & Mika, A. Methods of the analysis of oxylipins in biological samples. *Molecules 2020, Vol. 25, Page 349* **25**, 349 (2020).
96. Ovčačíková, M., Lísa, M., Cífková, E. & Holčapek, M. Retention behavior of lipids in reversed-phase ultrahigh-performance liquid chromatography–electrospray ionization mass spectrometry. *J Chromatogr A* **1450**, 76–85 (2016).
97. Nouwade, K., Tfaili, S. & Chaminade, P. Investigation of stationary phases performance for eicosanoids profiling in RP-HPLC. *Anal Bioanal Chem* **413**, 6551–6569 (2021).
98. Hagn, G. *et al.* Plasma instead of serum avoids critical confounding of clinical metabolomics studies by platelets. *J Proteome Res* (2024).
99. Cebo, M., Fu, X., Gawaz, M., Chatterjee, M. & Lämmerhofer, M. Enantioselective ultra-high performance liquid chromatography-tandem mass spectrometry method based on sub-2μm particle polysaccharide column for chiral separation of oxylipins and its application for the analysis of autoxidized fatty acids and platelet releasates. *J Chromatogr A* **1624**, 461206 (2020).

100. Edmond de Hoffmann, V. S. *Mass Spectrometry: Principles and Applications*. (Wiley, 2007).
101. Lee, H. C. & Yokomizo, T. Applications of mass spectrometry-based targeted and non-targeted lipidomics. *Biochem Biophys Res Commun* **504**, 576–581 (2018).
102. Newman, J. W. *et al.* Esterified Oxylipins: Do They Matter? *Metabolites* **12**, 1007 (2022).
103. Ianevski, A., Giri, A. K. & Aittokallio, T. SynergyFinder 3.0: an interactive analysis and consensus interpretation of multi-drug synergies across multiple samples. *Nucleic Acids Res* **50**, W739–W743 (2022).
104. Evans, D. M. *et al.* Exposure time versus cytotoxicity for anticancer agents. *Cancer Chemother Pharmacol* **84**, 359–371 (2019).
105. Cui, Y. *et al.* Nordihydroguaiaretic acid restores expression of silenced E-cadherin gene in human breast cancer cell lines and xenografts. *Anticancer Drugs* **19**, 487–494 (2008).
106. Sui, X. *et al.* RSL3 Drives Ferroptosis Through GPX4 Inactivation and ROS Production in Colorectal Cancer. *Front Pharmacol* **9**, (2018).
107. Calder, P. C. Dietary arachidonic acid: harmful, harmless or helpful? *Br J Nutr* **98**, 451–453 (2007).
108. Pai, R., Tarnawski, A. S. & Tran, T. Deoxycholic acid activates β-catenin signaling pathway and increases colon cell cancer growth and invasiveness. *Mol Biol Cell* **15**, 2156–2163 (2004).
109. Hildreth, K., Kodani, S. D., Hammock, B. D. & Zhao, L. Cytochrome P450-derived linoleic acid metabolites EpOMEs and DiHOMEs: a review of recent studies. *J Nutr Biochem* **86**, 108484 (2020).
110. Wu, Q. *et al.* Soluble epoxide hydrolase inhibitor (TPPU) alleviates ferroptosis by regulating CCL5 after intracerebral hemorrhage in mice. *Biomed Pharmacother* **172**, 116301 (2024).
111. Lv, X. *et al.* Cytochrome P450 ω-hydroxylase inhibition reduces cardiomyocyte apoptosis via activation of ERK1/2 signaling in rat myocardial ischemia-reperfusion. *Eur J Pharmacol* **596**, 118–126 (2008).
112. Koppula, P., Zhuang, L. & Gan, B. Cytochrome P450 reductase (POR) as a ferroptosis fuel. *Protein Cell* **12**, 675 (2021).
113. Li, J. *et al.* An omega-3 polyunsaturated fatty acid derivative, 18-HEPE, protects against CXCR4-associated melanoma metastasis. *Carcinogenesis* **39**, 1380–1388 (2018).
114. Panigrahy, D., Greene, E. R., Pozzi, A., Wang, D. W. & Zeldin, D. C. EET signaling in cancer. *Cancer Metastasis Rev* **30**, 525 (2011).
115. Stanford, K. I. *et al.* 12,13-diHOME: An Exercise-Induced Lipokine that Increases Skeletal Muscle Fatty Acid Uptake. *Cell Metab* **27**, 1111-1120.e3 (2018).
116. Kiyama, T. *et al.* Essential roles of mitochondrial biogenesis regulator Nrf1 in retinal development and homeostasis. *Mol Neurodegener* **13**, 1–23 (2018).
117. Morin, C., Sirois, M., Echave, V., Rizcallah, E. & Rousseau, E. Relaxing effects of 17(18)-EpETE on arterial and airway smooth muscles in human lung. *Am J Physiol Lung Cell Mol Physiol* **296**, 130–139 (2009).
118. Balderas, E., Zhang, J., Stefani, E. & Toro, L. Mitochondrial BKCa channel. *Front Physiol* **6**, 135862 (2015).

119. Gurtovenko, A. A. & Anwar, J. Modulating the Structure and Properties of Cell Membranes: The Molecular Mechanism of Action of Dimethyl Sulfoxide. *Journal of Physical Chemistry B* **111**, 10453–10460 (2007).

7. Appendix

Table A 1: Abundancies of analytes of A2780 whole cell lysates (initial condition, control cells) and A2780 Mitochondria lysates (control cells)

Analyte	log2(nAUC) + 20		Analyte	log2(nAUC) + 20	
	Whole cell	Mitochondria		Whole cell	Mitochondria
AA	25,20283	19,34838	7-HDoHE	17,43486	NF
DHA	25,0244	21,21794	12-HEPE	17,42408	NF
Deoxycholic Acid	23,77823	21,85819	5-HpETE	17,4221	16,39906
Oleic Acid	23,54688	19,88876	7(8)-DiHDPA	17,27914	NF
DGLA / isoform II	22,89733	17,78056	a-Linolenic Acid	17,18794	NF
EPA	22,77812	16,53728	11(12)-DiHETE	16,84322	15,96031
DPA / isoform I	21,7076	17,48717	PGD2	16,61697	16,00172
4-HDoHE	21,25501	16,45458	14-HEPE	16,59275	NF
5-HETrE	21,1913	15,66066	11(12)-EET	16,48767	14,8716
DPA	21,16979	17,03729	12,13-DiHOME	16,44816	19,38355
5(6)-EET	20,99907	16,22831	PGA2	16,05806	16,82403
12-HETE / 8-HETE	20,51949	NF	22-HDoHE	16,01946	12,81476
8(9)-EET	20,32664	NF	19-HETE	15,97997	NF
5-HETE	20,27484	15,19303	11-HEPE	15,87595	NF
15-HETE	20,17203	15,05729	14,15-DiHETrE	15,83383	NF
DGLA	20,10561	15,89628	Glycolithocholic	15,63332	NF
17(18)-EpETE	20,00379	14,26316	Glycodeoxycholic	15,60381	NF
18-HEPE	19,98164	16,18711	11b-	15,50417	NF
DHA / isoform I	19,91937	14,5043	9,10-DiHOME	15,36866	18,09295
Adrenic Acid	19,75795	16,38694	18-HETE	15,18429	NF
Adrenic Acid / isoform II	19,73199	NF	19(20)-DiHDPA	14,9942	12,70788
Linoleic Acid	19,58483	18,88389	PGE2	14,73755	14,94518
8-HDoHE	19,55727	15,53682	HHTrE / isoform V	14,56736	13,52164
Palmitic Acid	19,52237	19,22099	11b-	14,52767	NF
9-HETE	19,49801	14,4635	Glycocholic Acid	13,98809	NF
14(15)-EpETE	19,32823	NF	16(17)-DiHDPA	13,05652	NF
PGE1	19,32512	16,22701	15deoxy-PGJ2	NF	19,29842
9- and 13-HODE_9(10)- and	19,24589	17,68483	HpODE / isoform	NF	17,93828
13-OxoODE	19,24505	15,38928	5,15-DiHETE	NF	17,07778
20-HDoHE	19,19493	14,60623	14(15)-DiHETE	NF	17,05304
5-Oxo-ETE	19,12362	NF	9-HpODE	NF	17,01885
4-HETE	19,06503	15,27448	Resolvin E4	NF	16,89888
14-HDPA	19,05354	15,42961	Lipoxin A4	NF	16,30127
13-, 16- and 17-HDoHE	18,8366	14,57669	Hepoxilin A3	NF	16,09984
8(9)-EpETE	18,71258	18,74828	13-, 16- and 17-	NF	15,58096
14-HDoHE / 10-HDoHE	18,62326	15,25823	HpODE / isoform	NF	15,53162
11-HETE	18,61612	14,69899	13-HpODE	NF	15,52578
14(15)-EET	18,50644	16,33505	9-HEPE	NF	15,1412
11(12)-EpETE	18,25342	18,15131	20-HEPE	NF	15,11732
13-HDPA	18,21511	15,42131	8,9-DiHETrE	NF	15,04085
5,6-DiHETrE	18,1372	13,82436	Lipoxin B4	NF	14,91102
g-Linolenic Acid	17,95993	13,53854	9-HOTrE	NF	14,54528
15-HETrE	17,9424	15,09444	13-HOTrE	NF	14,0749
EPA / isoform I	17,80231	14,56084	12-HETrE	NF	13,99235
Hepoxilin B3	17,74207	NF	13-HOTrE_gamma	NF	13,81768
5-HEPE	17,7248	15,83209	15-HEPE	NF	13,80046
11-HETrE	17,59841	NF	20-hydroxy-LTB4	NF	13,3729

Stearic Acid	17,58322	16,61299	g-Linolenic Acid /	NF	13,15653
20-HETE	17,52642	NF	A1-Phytoprostane-	NF	12,91173
11-HDoHE	17,43518	13,47842	a-Linolenic Acid /	NF	11,07177

Table A 2: List of all identified analytes in each A2780 whole cell and mitochondrial lysate and number of identified analytes per experiment, analytes only found in mitochondria are marked in yellow.

		A2780 Whole cell lysates		
	A2780 Mitochondria	Initial extraction	Optimization	Adjusted conditions
10(11)-DiHDPA				✓
11(12)-DiHETE	✓	✓		✓
11,12-DiHETrE			✓	✓
11b-PGE2				✓
11(12)-EET	✓	✓	✓	
11(12)-EpETE	✓	✓		
11b-PGF2a/PGF2b I		✓		
11b-PGF2a/PGF2b II		✓		✓
11-HDoHE	✓	✓		
11-HEPE		✓	✓	✓
11-HETE	✓	✓	✓	✓
11-HETrE		✓	✓	✓
12,13-DiHOME	✓	✓	✓	✓
12-HEPE		✓	✓	✓
12-HETE / 8-HETE		✓	✓	✓
12-HETrE	✓		✓	✓
13(14)-DiHDPA				✓
13-, 16- and 17-HDoHE	✓		✓	✓
13,14-dihydro-15-keto-PGE2			✓	
13-HDPA	✓	✓	✓	✓
13-HOTrE	✓			
13-HOTrE_gamma	✓		✓	
13-HpODE	✓		✓	✓
13-OxoODE	✓	✓	✓	✓
14(15)-DiHETE	✓			
14(15)-EET	✓	✓		
14(15)-EpETE		✓		
14(15)-DiHETE			✓	
14,15-DiHETrE		✓	✓	✓
14-HDoHE / 10-HDoHE	✓	✓	✓	
14-HDPA	✓	✓	✓	
14-HEPE		✓		✓
15deoxy-PGJ2	✓		✓	✓
15-HEPE	✓		✓	
15-HETE	✓	✓	✓	✓
15-HETrE	✓	✓	✓	
16(17)-DiHDPA		✓		✓
17(18)-EpETE	✓	✓	✓	✓
17-HETE				✓
18-HEPE	✓	✓	✓	✓
18-HETE		✓	✓	

19(20)-DiHDPA	✓	✓	✓	✓
19-HETE		✓		✓
20-HDoHE	✓	✓	✓	✓
20-HEPE	✓		✓	✓
20-HETE		✓	✓	✓
20-hydroxy-LTB4	✓			✓
22-HDoHE	✓	✓	✓	
4-HDoHE	✓	✓	✓	
4-HETE	✓	✓		
5(6)-EET	✓	✓	✓	✓
5,15-DiHETE	✓		✓	✓
5,6-DiHETrE	✓	✓	✓	
5-HEPE	✓	✓	✓	
5-HETE	✓	✓	✓	✓
5-HETrE	✓	✓	✓	✓
5-HpETE	✓	✓	✓	
5-Oxo-ETE		✓	✓	
7(8)-DiHDPA		✓	✓	✓
7-HDoHE		✓		
8(9)-EET		✓	✓	✓
8(9)-EpETE	✓	✓		✓
8,9-DiHETrE	✓		✓	
8-HDoHE	✓	✓		
9- and 13-HODE_9(10)- and 12(13)-EPOME	✓	✓	✓	
8-HEPE				✓
9,10-DiHOME	✓	✓	✓	✓
9-HEPE	✓		✓	✓
9-HETE	✓	✓	✓	✓
9-HOTrE	✓			
9-HpODE	✓		✓	✓
A1-Phytoprostane-I	✓			
AA	✓	✓	✓	✓
Adrenic Acid	✓	✓	✓	✓
Adrenic Acid / isoform II	✓	✓		
a-Linolenic Acid		✓		
a-Linolenic Acid / isoform I	✓			
Deoxycholic Acid	✓	✓	✓	✓
DGLA	✓	✓	✓	✓
DGLA / isoform II	✓	✓	✓	
DHA	✓	✓	✓	
DHA / isoform I	✓	✓		
DPA	✓	✓	✓	✓
DPA / isoform I	✓	✓	✓	
DPA / isoform II			✓	
EPA	✓	✓	✓	✓
EPA / isoform I	✓	✓		
EPA / isoform II			✓	
EPA / isoform IV			✓	
g-Linolenic Acid	✓	✓	✓	✓
g-Linolenic Acid / isoform I	✓		✓	
Hepoxilin A3	✓			
Glycocholic Acid		✓	✓	
Glycodeoxycholic Acid		✓	✓	
Glycolithocholic Acid		✓		

Hepoxilin B3		✓	✓	
HHTrE / isoform V	✓	✓		
HpODE / isoform III	✓		✓	
HpODE / isoform VI	✓		✓	
Linoleic Acid	✓	✓		✓
Lipoxin A4	✓		✓	✓
Lipoxin B4	✓			✓
Oleic Acid	✓	✓	✓	✓
Palmitic Acid	✓	✓		✓
PGA2	✓	✓	✓	✓
PGA3				✓
PGB3			✓	
PGD2	✓	✓		✓
PGE2				✓
PGE1	✓	✓		✓
PGE2	✓	✓		✓
PGF2a			✓	
Resolvin E4	✓			✓
Stearic Acid	✓	✓	✓	✓
Number of identified analytes	77	75	73	63